

Preprint of D.T Schoeffler and J.E. Shepherd, "Decay of plane shock waves in equilibrium flows," *Journal of Fluid Mechanics*, Vol. 1015, A41, 2025. See <https://doi:10.1017/jfm.2025.10355> for final version.

# Decay of plane shock waves in equilibrium flows

Donner T. Schoeffler<sup>1†</sup> and Joseph E. Shepherd<sup>1</sup>

<sup>1</sup>Graduate Aerospace Laboratories, California Institute of Technology, Pasadena, CA 91125, USA

A new model is presented for the decay of plane shock waves in equilibrium flows with an arbitrary equation of state. A fundamental challenge for the accurate prediction of shock propagation using analytical modeling is to account for the coupling between a shock's motion and the post-shock flow. Our model accomplishes this by neglecting only higher-order perturbations to the second velocity gradient,  $u_{xx}$ , in the incident simple wave. The second velocity gradient is generally small and exactly zero for centered expansion waves in a perfect gas, so neglecting its effect on the shock motion provides an accurate closure criterion for a shock-change equation. This second-order shock-change equation is derived for a general equation of state. The model is tested by comparison with numerical simulations for three problems: decay by centered waves in a perfect gas, decay by centered waves in equilibrium air, and decay by the simple wave generated from the constant deceleration of piston in a perfect gas. The model is shown to be exceptionally accurate for a wide range of conditions, including small  $\gamma$  and large shock Mach numbers. For a Mach 15 shock in equilibrium air, model errors are less than 2% in the first 60% of the shock's decay. The analytical results possess a simple formulation but are applicable to fluids with a general equation of state, enabling new insight into this fundamental problem in shock wave physics.

**Key words:**

---

## 1. Introduction

Shock decay is fundamental to numerous problems in fluid mechanics, resulting from either the geometric or unsteady expansion of the post-shock flow. Geometric effects have been famously modeled by Whitham's geometric shock dynamics (Whitham 1999, Chapter 8). However, predicting shock decay from the interaction with an unsteady wave in a general medium remains a challenging problem to describe analytically because a shock's motion is coupled with the post-shock flow. Predictive models for this wave interaction are important because it is fundamental to many problems in shock wave physics. In detonation physics, it is essential to the unsteady shock front of gaseous detonations (Jackson & Short 2013), to critical phenomena like minimum ignition energy (Eckett *et al.* 2000), and to the operation of detonation-driven shock tubes (Jiang *et al.* 2002). The interaction causes the shock attenuation in experiments using flyer plates (Fowles 1960) and laser-driven shocks (Cottet & Romain

<sup>†</sup> Email address for correspondence: dschoeff@caltech.edu

1982). Application of geometric methods to problems like spherical blast wave propagation is substantially complicated by the unsteady wave interaction (Best 1991). The interaction of an unsteady expansion with a shock is isolated for plane shock waves in equilibrium flows, and so this problem is the focus of the present article. With modern computational methods it is straightforward to directly simulate these one-dimensional shock dynamics, however, analytical methods remain essential for physical insight, time-efficient solutions, and analysis of experimental and computational data.

Many shock propagation theories have been developed over nearly a hundred years of research. A common analytical approach is to specify the conservation equations to the shock discontinuity and combine them with the Rankine-Hugoniot equations. A single equation can be derived, and early formulations by Cassen & Stanton (1948) and Chen & Gurtin (1971) showed how shock acceleration is determined by the balance of the post-shock pressure gradient with geometric divergence or chemical reaction, respectively. The resulting equation is often unnamed but sometimes referred to as the shock-change equation (Fickett & Davis 1979) or as singular surface theory (Wright 1976). A family of shock-change equations can be derived that relate shock acceleration to a derivative of any post-shock flow variable (Radulescu 2020). For one-dimensional equilibrium flows, predicting a shock's motion from these equations requires an additional condition on the post-shock flow, and this condition is typically what distinguishes different shock propagation theories and determines their accuracy for a given problem. Taylor (1939) developed a first theory by approximating the post-shock pressure gradient as constant. Chandrasekhar (1943) obtained a solution for weak shock pulses by assuming the velocity and sound speed to be spatially linear. Friedrichs (1948) first solved the problem of a weak plane shock decayed by a centered expansion in a perfect gas. This specific problem has seen significant attention since it is the simplest formulation for a shock decayed by an unsteady wave. Burnside & Mackie (1965) specifically analyzed the initial decay rate of the shock. Ardavan-Rhad (1970) and Sharma *et al.* (1987) developed models also assuming linearity of the post-shock velocity distribution. Fowles (1960) derives a similar theory to Friedrichs using a Murnaghan equation of state. For general one-dimensional shocks (planar, cylindrical, and spherical), Brinkley & Kirkwood (1947) derived a second-order shock propagation equation using a condition on the similarity of shock energy over time. Many other theories have come from efforts to model the non-self-similar motion of blast waves when the shock strength is finite and the upstream pressure is nonzero. These theories are not reviewed here but are described in monographs by Korobeinikov (1991), Sachdev (2004), and Lee (2016), which also discuss some of the other theories above.

The shock-change equation formalism was also used by Chester (1954), Chisnell (1957), and Whitham (1958) to model the effect of a nonuniform upstream medium on a shock's motion, particularly due to quasi-one-dimensional area changes. They neglected the coupling between the shock's motion and the post-shock flow, which is equivalent to assuming that all incoming  $C^+$  characteristics originate from a region of uniform flow. Whitham developed the theory into his shock dynamics (Whitham 1999, Chapter 8) and identified that the method's fundamental assumption is

$$\partial_t P + \rho a \partial_t u = 0 \quad (1.1)$$

at the shock front, where  $P$  is the pressure,  $\rho$  is the density,  $a$  is the sound speed, and  $u$  is the particle velocity. The approximation has enabled expedient and reasonably accurate estimation of shock motion for a wide range of problems. However, for problems with rapid geometric expansion, such as in blast waves and shock diffraction (Skews 1967), coupling with the post-shock flow cannot be ignored and so the accuracy of (1.1) is worse. The effect of incoming disturbances on Chester-Chisnell-Whitham (CCW) theory was studied by

Rościszewski (1960), Oshima *et al.* (1965), and Yousaf (1974, 1982), and *ad hoc* methods (Ridoux *et al.* 2019) have been developed to remedy this issue for numerical implementations of geometric shock dynamics (Henshaw *et al.* 1986). Best (1991) sought to include the effect of incoming disturbances by extending the approximation (1.1) to higher orders.

Shock propagation theories are not limited to approximations on first-order post-shock derivatives but can be formulated for any higher-order derivative. If a shock-change equation is derived for each term in the series expansion of a dependent variable, then an infinite hierarchy of equations can be obtained, and truncation of the series expansion provides a sufficient condition to solve all lower-order equations. Friedlander (1958) presents this theory in detail for sound pulses, where higher-order equations provide corrections to geometric acoustics. Similarly, since geometric shock dynamics is obtained from (1.1), Best (1991) derived higher-order corrections using a series expansion in terms of

$$\partial_t^{n-1}(\partial_t P + \rho a \partial_t u) = 0. \quad (1.2)$$

An alternative approach is given by Sharma & Radha (1994), who use a series expansion in space of the post-shock pressure, so that truncation at order  $n$  is given by

$$\partial_x^n P = 0. \quad (1.3)$$

Although arbitrarily higher-order shock propagation equations can be derived, enabling in principle arbitrarily accurate solutions, the utility of these methods is limited because higher-order equations become exceedingly cumbersome to derive and the accuracy achievable at any given order is not clear. Additionally, higher-order equations require initial conditions at every lower order. These initial conditions cannot be arbitrary, since they must be compatible with a series expansion of a solution to the governing equations. Obtaining these initial conditions is itself a difficult problem.

The difficulty of these higher-order theories is highlighted for the problem of plane shock decay. Plane shock waves in a uniform medium can only decay from the interaction with a simple wave, which entirely determines the resulting shock motion. In the simplest case, the wave is self-similar and centered, and a space-time diagram for the interaction with a shock is shown in figure 1. The shock interaction generates a wave propagating along  $C^-$  characteristics, which perturbs the post-shock flow from purely the incident simple wave. For an arbitrary flow variable,  $q$ , the perturbed quantity in the post-shock flow can be written simply as

$$q = q^{(0)} + q^{(1)}, \quad (1.4)$$

where  $q^{(0)}$  is given by the unperturbed incident simple wave and  $q^{(1)}$  is the perturbation. An infinite hierarchy of shock-change equations can be obtained by a series expansion of  $q$  at the shock front. The series expansion can be truncated to solve the system of equations, however this introduces truncation error not only from the perturbation, but also the incident wave. Instead, if only the series expansion for the perturbation is truncated,

$$\partial_x^n q^{(1)} = 0, \quad (1.5)$$

then the system of equations can be solved including the effect of the unperturbed simple wave at all orders. The problem is then reduced to identifying the appropriate variable to use for  $q$  and obtaining initial conditions for the perturbed wave. The subject of this article is the development, implementation, and validation of this theory for the decay of plane shocks.

Since shock wave phenomena are important in many diverse media, an important point is that theories using the shock-change equation formalism can be derived for a general equation of state. This has been used before by some authors. Brinkley & Kirkwood (1947) derive their theory for a general equation of state, Best (1991) implements a Tait equation of

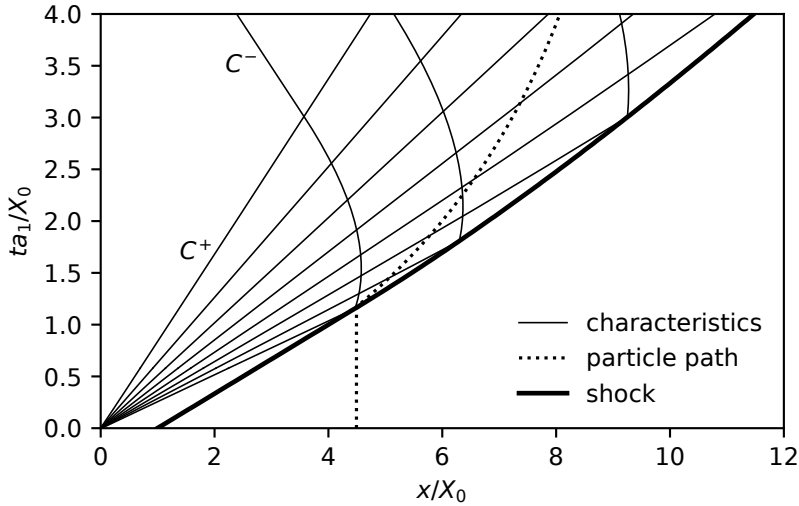


Figure 1: Space-time diagram of a shock decayed by a centered expansion wave. This diagram was generated from numerical simulation results presented later in this work for a Mach 3 shock and isentropic exponent  $\gamma = 1.4$ .  $X_0$  is the shock's initial distance from the origin, and  $a_1$  is the upstream sound speed

state, and Singh & Arora (2021) applied Sharma & Radha's theory to a van der Waals gas. However, most prior work only considers a perfect gas model. The theory presented in this article is derived for a general equation of state.

The structure of this article is as follows. In section 2, the problem of a shock decayed by an arbitrary simple wave is formulated. From analysis of the simple wave motion, it will be shown that an optimal truncation term is the second gradient of velocity,  $u_{xx}$ , which is identically zero throughout a centered expansion in a perfect gas. The shock-change equation for  $u_{xx}$  is derived in section 3. The derivation is developed by defining coefficients for each first-order shock-change equation, which enables a compact presentation of the second-order results. The second-order ordinary differential equation and strong and weak shock solutions are discussed in section 4. In order to implement the shock decay model for any given simple wave interaction, the initial shock decay rate is required. A solution for the perturbed initial condition is given in section 5. Finally, section 6 presents the major results of this article, where the present model is compared with numerical simulations and several prior theories.

## 2. Formulation

An initially steady plane shock wave decays when overtaken by a simple expansion wave. The properties of the expansion wave determine the rate of decay of the shock over time. Any simple wave can be modeled as having originated from the motion of some piston. If a piston impulsively accelerates to speed  $u_2$  and impulsively stops after time  $\tau_p$ , then a shock with speed  $U_0$  is driven ahead of a centered expansion wave that overtakes the shock at later time. Figure 1 depicts the resulting space-time diagram for a Mach 3 shock, where the time when the piston stops is  $t = 0$ . Coordinates are scaled by the shock position when the piston stops, which is given by

$$X_0 = (U_0 - u_2)\tau_p. \quad (2.1)$$

The space-time diagram shows the  $C^-$  characteristics of the reflected wave. The particle path drawn intersects the point at which the shock begins decaying and so bounds the region of nonuniform entropy behind the shock. The nonuniform entropy and reflected wave perturb the incident simple wave.

The theory of simple waves is discussed in many books, e.g., Thompson (1972) and Landau & Lifshitz (1987). The equations describing any simple wave for a general equation of state are

$$x = (u + a(u))t + f(u), \quad (2.2)$$

$$du - \frac{da}{\Gamma - 1} = 0 \quad \text{on } C^- \text{ characteristics}, \quad (2.3)$$

where  $f(u)$  is some function that satisfies the boundary conditions given by the piston motion and  $\Gamma$  is the fundamental derivative of gas dynamics (Thompson 1971).

If the piston is impulsively stopped, then all characteristics are centered at the stopping point and (2.2) becomes

$$x = (u + a(u))t. \quad (2.4)$$

Equation (2.4) is also obtained asymptotically from (2.2) as  $t \rightarrow \infty$ , because on a given  $C^+$  characteristic  $f(u)$  is constant and so becomes much smaller than  $(u + a(u))t$ . Using (2.3), the velocity gradient in the centered wave is given by

$$u_x = \frac{1}{\Gamma t}, \quad (2.5)$$

which shows that  $u_x$  is spatially uniform, except for any variation in  $\Gamma$ . If the medium is a perfect gas, then  $\Gamma = (\gamma + 1)/2$  is constant, where  $\gamma$  is the ratio of specific heat capacities, and the first and second velocity gradients are

$$u_x = \frac{2}{(\gamma + 1)t} \quad (2.6)$$

$$u_{xx} = 0. \quad (2.7)$$

The second gradient,  $u_{xx}$ , is exactly zero everywhere throughout the wave. From (2.3), it is straightforward to show that the second gradient of sound speed,  $a_{xx}$ , is also zero everywhere. Second order derivatives of all other dependent variables are nonzero. The temperature, pressure, and density throughout the wave are given by

$$\begin{aligned} T &= T_0 \left( \frac{a}{a_0} \right)^2, \\ P &= P_0 \left( \frac{a}{a_0} \right)^{\frac{2\gamma}{\gamma-1}}, \\ \rho &= \rho_0 \left( \frac{a}{a_0} \right)^{\frac{2}{\gamma-1}}, \end{aligned} \quad (2.8)$$

where the subscript 0 denotes a reference state in the isentropic flow. For values of  $\gamma$  where  $n = 2\gamma/(\gamma - 1)$  is an integer, then the lowest-order gradients of  $T$ ,  $P$ , and  $\rho$  to vanish are

$$\partial_x^3 T = 0, \quad (2.9)$$

$$\partial_x^{n+1} P = 0, \quad (2.10)$$

$$\partial_x^{n-1} \rho = 0. \quad (2.11)$$

For  $\gamma = 5/3$ ,  $n = 5$ , and for  $\gamma = 7/5$ ,  $n = 7$ . In Best's truncation term (1.2), partial derivatives with respect to time are used. For all second order derivatives, including mixed partials, only  $u_{xx}$  and  $a_{xx}$  are zero. This can be seen by suitably differentiating (2.4) and (2.8).

For a centered expansion in a perfect gas,  $u_{xx}$  and  $a_{xx}$  can only be nonzero behind a decaying shock due to the perturbation by reflected waves. The proposed model is to neglect this perturbation and apply  $u_{xx} = 0$  at the shock, which is a sufficient condition to obtain a second-order shock propagation equation. The term  $u_{xx}$  is chosen over  $a_{xx}$  due to the simpler derivation and because it is continuous through jumps in the entropy gradient, such as across the particle path in figure 1. Note that this model is only applied in the limit approaching the shock position from behind, and so it is independent of discontinuities in  $u_{xx}$ , e.g., at the head of the reflected wave.

For an arbitrary simple wave in a general medium,  $u_{xx} \neq 0$ , and so this variation must be accounted for. If  $\Gamma$  is not constant, then

$$\frac{u_{xx}}{u_x^2} = -\frac{\Gamma - 1}{\Gamma} \partial_a \Gamma, \quad (2.12)$$

where  $\partial_a \Gamma$  is the variation of  $\Gamma$  with the equilibrium sound speed at constant entropy. For many cases, (2.12) may be sufficiently small that it can be neglected, for example, this will be shown for equilibrium air. In cases where this approximation cannot be made, then the  $u_{xx}$  in the unperturbed incident wave must be evaluated for each characteristic.

If the piston slows to a halt monotonically but its motion is otherwise general, then  $u_x$  and  $u_{xx}$  are given by

$$u_x = \frac{1}{\Gamma t + f'(u)}, \quad (2.13)$$

$$u_{xx} = -\left(\frac{\partial \Gamma}{\partial a}\right)_s (\Gamma - 1)t + f''(u) u_x^3, \quad (2.14)$$

and, for a perfect gas,

$$\frac{u_{xx}}{u_x^2} = -\frac{f''(u)}{(\gamma + 1)t/2 + f'(u)}. \quad (2.15)$$

By neglecting only the perturbation to  $u_{xx}$  by reflected waves, the unperturbed value given by (2.15) can still be used to evaluate  $u_{xx}$  at the shock. However, as discussed previously, the simple wave from a general piston deceleration rapidly approaches the self-similar centered expansion as time advances. So, an additional approximation is to still apply  $u_{xx} = 0$  at the shock and use (2.15) to estimate the additional induced error. This is equivalent to approximating the incident simple wave as a centered expansion with an equivalent initial velocity gradient  $u_x$ , which determines the initial shock decay rate.

The tendency toward a self-similar solution is a feature of many fluid mechanics problems, including shock propagation. Strong decaying shocks over sufficiently large time approach a self-similar limit described by Zel'dovich & Raizer (1967). In this limit,  $u_{xx}$  again equals zero, including behind the decaying shock, even if  $u_{xx} \neq 0$  initially from a general piston motion and the reflected perturbation. Uniformity of the velocity gradient in self-similar flows is a property discussed by Pert (1980) and motivated the work by Sharma *et al.* (1987). Indeed, Chandrasekhar (1943) and Ardavan-Rhad (1970) both also use similar models. The difference here is that  $u_{xx}$  is assumed to be zero only at the shock front, and no assumptions are made about the flow further behind the shock.

This shock decay model will be compared with numerical simulations to test the three factors that cause  $u_{xx}$  to deviate from zero. First, simulations of shocks decayed by a centered expansion in a perfect gas will evaluate the magnitude of the perturbation by the shock

interaction, since  $u_{xx}^{(0)} = 0$  exactly. Second, simulations of shocks decayed by a centered expansion in equilibrium air will provide one example of a general equation of state that significantly departs from a perfect gas. Third, simulations of shocks decayed by the simple wave generated from the constant deceleration of the piston will examine the departure from  $u_{xx}^{(0)} = 0$ .

### 3. Shock-change equations

The aim of the following derivation is to obtain the shock-change equation that relates plane shock motion with post-shock values of  $u_{xx}$ . Aspects of the derivation appear in many previous articles, including recent work (Radulescu 2020). However, other than the main results, a useful feature of the present derivation is the formalism of defining coefficients for each shock-change equation. These coefficients can be evaluated independent of any problem and provide a substantially more compact approach for deriving higher-order shock-change equations for a general equation of state. In this work, equilibrium flow is specified throughout because nonequilibrium phenomena, such as vibrational relaxation or exothermic chemical reaction, are also coupled with the shock motion. These effects are included in many shock-change equation derivations (Fickett & Davis 1979; Sharma & Radha 1994), however they are beyond the scope of the present work. Equilibrium flow assumes that the time scale of these phenomena is either much greater or smaller than characteristic flow time scales. Vincenti & Kruger (1965) describe equilibrium flows in detail.

The equations of motion for equilibrium flow in one dimension, neglecting diffusion of mass, momentum, and energy, are

$$\frac{D\rho}{Dt} + \rho \frac{\partial u}{\partial x} = 0, \quad (3.1)$$

$$\frac{Du}{Dt} + \frac{1}{\rho} \frac{\partial P}{\partial x} = 0, \quad (3.2)$$

$$\frac{DP}{Dt} - a^2 \frac{D\rho}{Dt} = 0, \quad (3.3)$$

where  $a$  is the equilibrium sound speed. An equation of state closes the system and can be specified generally, for example, as  $a = a(P, \rho)$ . It is useful as a first step to combine the continuity and energy equation, which gives

$$\frac{DP}{Dt} + \rho a^2 \frac{\partial u}{\partial x} = 0. \quad (3.4)$$

Consider a shock propagating with speed  $U(t)$  and position  $X(t)$  into an otherwise uniform flow with conditions given by  $u_1$ ,  $P_1$ , and  $\rho_1$ , where subscript 1 denotes the upstream state. The derivation in the case of a nonuniform upstream flow is given by Schoeffler & Shepherd (2023a). Although the shock is unsteady, the discontinuous jump in flow variables can still be found by control volume analysis and is given instantaneously at all time by the Rankine-Hugoniot equations,

$$\rho_2 w_2 = \rho_1 w_1, \quad (3.5)$$

$$P_2 + \rho_2 w_2^2 = P_1 + \rho_1 w_1^2, \quad (3.6)$$

$$h_2 + w_2^2/2 = h_1 + w_1^2/2, \quad (3.7)$$

where subscript 2 denotes the post-shock state,  $h$  is the enthalpy, and  $w$  is the flow velocity in the shock-fixed frame, i.e.,  $w = U - u$ . With an equation of state, the Rankine-Hugoniot

equations can be solved for the post-shock state, where each quantity can be written generally as

$$\begin{aligned} w_2 &= w_2(w_1, P_1, \rho_1), \\ P_2 &= P_2(w_1, P_1, \rho_1), \\ \rho_2 &= \rho_2(w_1, P_1, \rho_1), \\ a_2 &= a_2(P_2, \rho_2), \\ &= a_2(w_1, P_1, \rho_1). \end{aligned} \quad (3.8)$$

Assuming  $u_1 = 0$ , then  $w_1 = U(t)$ . Since  $w_1 = U(t)$  is not constant, the post-shock quantities are varying with time, and so the flow is nonuniform. The resulting gradients behind the shock are described by the conservation equations, (3.2) and (3.4), evaluated at the shock discontinuity, i.e.,

$$\begin{aligned} \left. \frac{Du}{Dt} \right|_2 + \frac{1}{\rho_2} \left. \frac{\partial P}{\partial x} \right|_2 &= 0, \\ \left. \frac{DP}{Dt} \right|_2 + \rho_2 a_2^2 \left. \frac{\partial u}{\partial x} \right|_2 &= 0. \end{aligned} \quad (3.9)$$

The time-variation of any post-shock variable can be obtained by differentiating (3.8), e.g., for the post-shock pressure,

$$\frac{dP_2}{dt} = \frac{\partial P_2}{\partial w_1} \dot{U}(t), \quad (3.10)$$

where  $\dot{U}(t)$  is the shock acceleration. The partial derivative coefficient is only a function of the shock Hugoniot and instantaneous shock speed. The time derivative of the post-shock quantity  $P_2$  is equivalent to a total derivative of the field variable evaluated at the shock's position,  $P(X(t), t)$ , i.e.,

$$\frac{dP_2}{dt} = \left. \frac{\partial P}{\partial t} \right|_2 + U(t) \left. \frac{\partial P}{\partial x} \right|_2. \quad (3.11)$$

This derivative is analogous to the material derivatives in the conservation equations and referred to as shock derivatives. Material derivatives can be expressed in terms of shock derivatives by

$$\left. \frac{D}{Dt} \right|_2 = \frac{d}{dt} + (u_2 - U) \left. \frac{\partial}{\partial x} \right|_2. \quad (3.12)$$

Applying (3.12) to the (3.9) gives

$$\begin{aligned} \frac{du_2}{dt} + (u_2 - U)u_{x,2} + \frac{P_{x,2}}{\rho_2} &= 0, \\ \frac{dP_2}{dt} + (u_2 - U)P_{x,2} + \rho_2 a_2^2 u_{x,2} &= 0, \end{aligned} \quad (3.13)$$

where subscript notation has been adopted for partial differentiation. The equations can now be combined to eliminate either the pressure or velocity gradient. Eliminating the pressure gradient and simplifying gives

$$\frac{dP_2}{dt} + \rho_2 w_2 \frac{du_2}{dt} + \rho_2 a_2^2 \eta u_{x,2} = 0, \quad (3.14)$$

where

$$\eta = 1 - \frac{w_2^2}{a_2^2}. \quad (3.15)$$

The shock derivatives can be expanded in terms of the shock acceleration by differentiating (3.8) as shown in (3.10). Equation (3.14) becomes

$$u_{x,2} = -\frac{1}{\rho_2 a_2^2 \eta} \left[ \frac{\partial P_2}{\partial w_1} + \rho_2 w_2 \frac{\partial u_2}{\partial w_1} \right] \dot{U}. \quad (3.16)$$

This result can be expressed compactly as

$$u_{x,2} = F \dot{M}, \quad (3.17)$$

where  $\dot{M} = \dot{U}/a_1$  and

$$F = -\frac{a_1}{\rho_2 a_2^2 \eta} \left[ \frac{\partial P_2}{\partial w_1} + \rho_2 w_2 \frac{\partial u_2}{\partial w_1} \right]. \quad (3.18)$$

The coefficient  $F$  is nondimensional and only a function of the shock Hugoniot. Equation (3.17) represents one of a family of shock-change equations that relate first-order derivatives of post-shock flow variables with the shock acceleration. All first-order shock-change equations can be expressed similarly in terms of a coefficient multiplying the shock acceleration to give any post-shock flow derivative.

Shock-change equations for all other post-shock flow derivatives can be derived using (3.17). The equation for the pressure gradient can be derived from the momentum equation (3.2),

$$\begin{aligned} \left. \frac{1}{\rho_1 a_1} \frac{\partial P}{\partial x} \right|_2 &= -\left. \frac{\rho_2}{\rho_1 a_1} \frac{Du}{Dt} \right|_2 \\ &= -\frac{\rho_2}{\rho_1 a_1} \left[ \frac{du_2}{dt} - w_2 \left. \frac{\partial u}{\partial x} \right|_2 \right] \\ &= -\frac{\rho_2}{\rho_1} \left[ \frac{\partial u_2}{\partial w_1} - \frac{w_2}{a_1} F \right] \dot{M} \\ &= G \dot{M}, \end{aligned} \quad (3.19)$$

where  $G$  is the corresponding coefficient for the pressure gradient. The shock-change equation for the density gradient can be obtained from (3.1) and is

$$\left. \frac{a_1}{\rho_1} \frac{\partial \rho}{\partial x} \right|_2 = H \dot{M} \quad (3.20)$$

$$H = \frac{a_1}{\rho_1 w_2} \left( a_1 \frac{\partial \rho_2}{\partial w_1} + \rho_2 F \right) \quad (3.21)$$

With  $G$  and  $H$ , coefficients for any other thermodynamic quantities can be derived using the equation of state. For example, the sound speed gradient is given by

$$\left. \frac{\partial a}{\partial x} \right|_2 = E \dot{M} \quad (3.22)$$

$$E = \rho_1 a_1 \left. \frac{\partial a}{\partial P} \right|_2 G + \frac{\rho_1}{a_1} \left. \frac{\partial a}{\partial \rho} \right|_2 H \quad (3.23)$$

where the partial derivative coefficients are thermodynamic functions.

All of the above are first-order shock-change equations. By differentiating the conservation equations, a similar procedure of substitution can be used to obtain higher-order shock-change

equations. The gradients of (3.2) and (3.4) are

$$\frac{\partial}{\partial x} \left( \frac{Du}{Dt} + \frac{1}{\rho} \frac{\partial P}{\partial x} \right) = 0, \quad (3.24)$$

$$\frac{\partial}{\partial x} \left( \frac{DP}{Dt} + \rho a^2 \frac{\partial u}{\partial x} \right) = 0. \quad (3.25)$$

Expanding the derivatives gives

$$u_{tx} + u_x^2 + uu_{xx} - \frac{1}{\rho^2} \rho_x P_x + \frac{1}{\rho} P_{xx} = 0, \quad (3.26)$$

$$P_{tx} + u_x P_x + u P_{xx} + \rho_x a^2 u_x + 2\rho a a_x u_x + \rho a^2 u_{xx} = 0, \quad (3.27)$$

and by re-expressing time derivatives as shock derivatives we have

$$\frac{du_x}{dt} - w u_{xx} + u_x^2 - \frac{1}{\rho^2} \rho_x P_x + \frac{1}{\rho} P_{xx} = 0, \quad (3.28)$$

$$\frac{dP_x}{dt} - w P_{xx} + u_x P_x + \rho_x a^2 u_x + 2\rho a a_x u_x + \rho a^2 u_{xx} = 0. \quad (3.29)$$

Eliminating  $P_{xx}$  gives a single equation,

$$\frac{dP_x}{dt} + \rho w \frac{du_x}{dt} + \rho w u_x^2 - \frac{w}{\rho} \rho_x P_x + u_x P_x + \rho_x a^2 u_x + 2\rho a a_x u_x + (\rho a^2 - \rho w^2) u_{xx} = 0. \quad (3.30)$$

The shock derivatives of post-shock gradients can be found from differentiating the first-order shock-change equations, i.e.,

$$\frac{1}{\rho_1 a_1} \frac{dP_{x,2}}{dt} = G' \dot{M}^2 + G \ddot{M}, \quad (3.31)$$

$$\frac{du_{x,2}}{dt} = F' \dot{M}^2 + F \ddot{M}, \quad (3.32)$$

where  $\ddot{M}$  is the second time derivative of the shock Mach number, and  $F'$  and  $G'$  are

$$F' = \frac{dF}{dM}, \quad G' = \frac{dG}{dM}. \quad (3.33)$$

Therefore, by replacing all post-shock gradients with their corresponding shock-change equation and grouping terms, equation (3.30) can be simply expressed as

$$\ddot{M} + K \dot{M}^2 + L a_1 u_{xx,2} = 0, \quad (3.34)$$

where  $K$  and  $L$  are second-order shock-change coefficients given by

$$K = \left[ G' + M F' + M F^2 - \frac{\rho_1^2}{\rho_2^2} M G H + F G + \frac{a_2^2}{a_1^2} H F + 2 \frac{\rho_2 a_2}{\rho_1 a_1} E F \right] (G + M F)^{-1}, \quad (3.35)$$

$$L = \frac{\rho_2 a_2^2}{\rho_1 a_1^2} \eta (G + M F)^{-1}. \quad (3.36)$$

Similar to the first-order results,  $K$  and  $L$  are nondimensional and valid for an arbitrary equation of state, where the only assumption has been that the flow is in thermodynamic equilibrium. Equation (3.34) is the desired second-order shock-change equation for  $u_{xx}$ .

Sharma & Radha (1994) instead formulate a second-order shock-change equation in terms

of  $P_{xx}$ , and Best (1991) uses  $\partial_t(P_t + \rho au_t)$ . These equations can be derived using (3.34). To obtain the equation for  $P_{xx,2}$ , (3.34) is substituted into (3.28), which gives upon simplification

$$\ddot{M} + J\dot{M}^2 + N\frac{P_{xx,2}}{\rho_1} = 0 \quad (3.37)$$

where the coefficients are

$$J = \frac{F' + M\frac{\rho_1 K}{\rho_2 L} + F^2 - \frac{\rho_1^2}{\rho_2^2} GH}{F + \frac{\rho_1 M}{\rho_2 L}}, \quad (3.38)$$

$$N = \frac{\rho_1}{\rho_2} \left( F + \frac{\rho_1}{\rho_2} \frac{M}{L} \right)^{-1}. \quad (3.39)$$

The coefficients for Best's formulation are more complex and therefore derived separately in Appendix A.5.

For a perfect gas, the equation of state is given by the ideal gas law, and the heat capacities are constant. All of the shock-change coefficients can be re-expressed as functions of only  $M$  and  $\gamma$ . Some of the coefficients are given here explicitly,

$$F = -\frac{2}{\gamma + 1} \frac{3M^2 + 1}{M(M^2 - 1)}, \quad (3.40)$$

$$G = -\frac{2(M^2 + 1)}{(\gamma - 1)M^2 + 2} - \frac{2(3M^2 + 1)}{(\gamma + 1)(M^2 - 1)}, \quad (3.41)$$

$$H = -\frac{2(\gamma + 1)M^2(3(\gamma - 1)M^4 - (\gamma - 3)M^2 + 2(\gamma + 2))}{(M^2 - 1)((\gamma - 1)M^2 + 2)^3}, \quad (3.42)$$

$$K = \frac{-3M((9\gamma - 7)M^4 + 10(\gamma + 1)M^2 - 3\gamma + 13)}{(M^2 - 1)((7\gamma - 5)M^4 + 2(\gamma + 5)M^2 - \gamma + 3)}, \quad (3.43)$$

$$L = -\frac{(\gamma + 1)(M^2 - 1)^2((\gamma - 1)M^2 + 2)}{2(7\gamma - 5)M^4 + 4(\gamma + 5)M^2 - 2\gamma + 6}. \quad (3.44)$$

The coefficient for the sound speed gradient,  $E$ , can be obtained from (3.23) using the perfect gas equation of state,

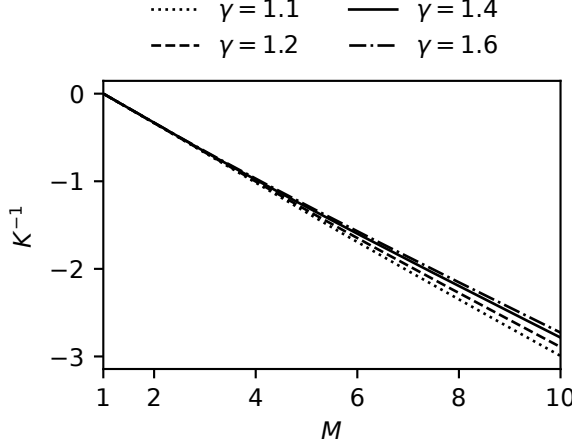
$$a = \sqrt{\gamma P / \rho}. \quad (3.45)$$

Each shock-change coefficient above is plotted for a range of  $M$  and  $\gamma$  in Appendix B.

#### 4. Shock decay model

For a known incident simple wave, the unperturbed second velocity gradient  $u_{xx,2}^{(0)}$  can be used to close the shock-change equation (3.34) and solve for the shock Mach number time evolution. As discussed in section 2,  $u_{xx,2}^{(0)} = 0$  exactly for centered expansion waves in a perfect gas and can be applied as a model for arbitrary simple waves with a general equation of state. By applying this to (3.34), then the following shock propagation equation is obtained

$$\begin{aligned} \ddot{M} + K\dot{M}^2 &= 0, \\ M(0) &= M_0, \\ \dot{M}(0) &= \dot{M}_0, \end{aligned} \quad (4.1)$$

Figure 2:  $K^{-1}$  for a range of  $M$  and  $\gamma$ 

where  $K = K(M)$  is given by (3.35) for a general equation of state and (3.43) for a perfect gas. The system of equations (4.1) describes an initial value problem, which can be numerically integrated for known initial conditions and equation of state to obtain the solution  $M(t)$ .

For a perfect gas, figure 2 shows that  $K^{-1}$  has a near linear dependence on  $M$ , which suggests approximating it as

$$K \approx K(M_0) \frac{M_0 - 1}{M - 1}, \quad (4.2)$$

where  $K(M_0)$  is the value of  $K$  at the initial condition. With this approximation, (4.1) can be integrated analytically, and the solution is

$$\delta(t) = \frac{1}{(1 + \beta t / \alpha)^\alpha}, \quad (4.3)$$

$$\delta(t) = \frac{M(t) - 1}{M_0 - 1}, \quad \beta = \frac{-\dot{M}_0}{M_0 - 1}, \quad \alpha = -\frac{1}{K(M_0)(M_0 - 1) + 1}.$$

The solution has the functional form of a power law, where the exponent  $\alpha$  is determined by the function  $K$ .  $\beta$  is the initial shock decay rate and provides the time scale for the shock's evolution.

The shock decay model (4.1) was integrated for a range of initial shock Mach numbers and  $\gamma$  using a fourth order Runge-Kutta scheme. The results are shown in figure 3 with the power-law approximation (4.3), where the time coordinate is scaled by the initial shock acceleration. Compared with numerically integrating (4.1), the approximate solution (4.3) is reasonably accurate with errors larger for increasing  $\gamma$  and  $M_0$ . For  $M_0 = 10$  and  $1 \leq \gamma \leq 5/3$ , the error given by the approximate solution when  $\delta = 0.4$  is less than 1.4%, and when  $\delta = 0.2$  it is less than 4.7%. Values for the power law exponent,  $\alpha$ , are plotted in figure 4.

The shock acceleration can be obtained by differentiating (4.3) and is

$$\frac{\dot{M}}{M_0 - 1} = \frac{-\beta}{(1 + \beta t / \alpha)^{\alpha+1}} \quad (4.4)$$

$$\tau_d = \left( \frac{-\dot{M}}{M - 1} \right)^{-1} = \frac{1}{\beta} + \frac{t}{\alpha}. \quad (4.5)$$

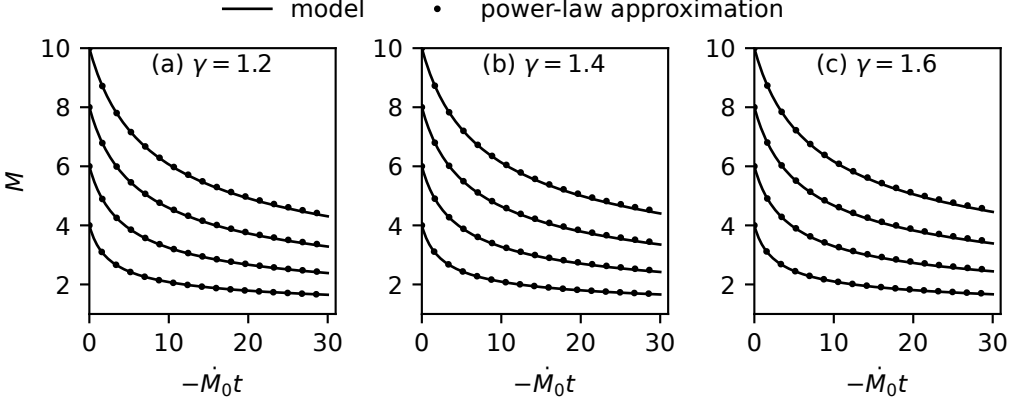


Figure 3: Shock decay model and its power-law approximate solution for a perfect gas with (a)  $\gamma = 1.2$ , (b)  $\gamma = 1.4$ , and (c)  $\gamma = 1.6$

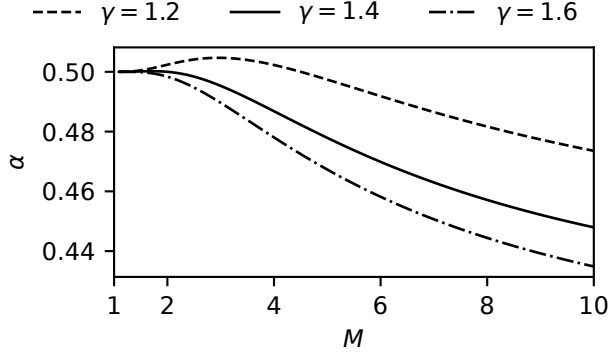


Figure 4: Variation in  $\alpha$  with  $M$  and  $\gamma$

The time scale of local unsteadiness for a particle processed by the decaying shock is given by  $\tau_d$ . Equation (4.5) shows that  $\tau_d$  increases linearly with time as the shock decays.

The weak shock limit for  $\alpha$  is obtained from a series expansion about  $M_0 = 1$  and is

$$\alpha = \frac{1}{2} + O((M_0 - 1)^4). \quad (4.6)$$

The leading-order term is the  $\frac{1}{2}$  power that is well known to be the solution for weak shock decay from Friedrichs (1948). Notably, this approximation is good to four orders in  $(M_0 - 1)$  and independent of  $\gamma$ .

The strong shock limit,  $1/M_0 \rightarrow 0$ , gives

$$\alpha = \frac{7\gamma - 5}{4(5\gamma - 4)} + O(M_0^{-2}), \quad (4.7)$$

where in this case  $\delta = M/M_0$  and  $\beta = -\dot{M}_0/M_0$ .

The power-law approximation has important correspondence with self-similar theories. Self-similar solutions typically apply in some asymptotic limit for a given problem (Barenblatt

& Zel'dovich 1972). For strong shocks, in the limit of large time, when  $\beta t/\alpha \gg 1$ , the typical formulation of self-similar shock propagation is obtained,

$$M \sim At^{-\alpha} \quad (4.8)$$

where  $A = M_0(\beta/\alpha)^{-\alpha}$  and  $\alpha$  is interpreted as the similarity exponent. In our model,  $\alpha$  for strong shocks is given by (4.7), which provides a good approximation for the similarity exponents reported by Zel'dovich & Raizer (1967) for the problem of an impulsive load (note that the exponent is defined differently here). The agreement is not surprising since the self-similar solution results in  $u_{xx} = 0$ , so the assumptions of the present model will yield exact results for such cases. This suggests that the general formulation for  $K$  could be used to obtain similarity exponents for other equations of state by examining the limit of  $M \rightarrow \infty$ .

The power-law approximation motivated recent work by the authors to model the decay of plane shocks in detonation-driven shock tubes (Schoeffler & Shepherd 2023b). The strong shock formulation was used to fit simulation data, where  $\alpha$  and  $\beta$  were instead used as fit parameters. The agreement was excellent and provided a method for quantifying shock decay for varying shock tube conditions.

## 5. Initial shock decay rate

When a simple wave first overtakes an initially steady shock, then the initial shock acceleration,  $\dot{M}_0$ , is required to implement the shock decay model (4.1). This quantity is not generally known and must be estimated. Rough estimates can be obtained by using a first-order shock-change equation with a gradient in the incident simple wave, however the first-order gradient is instantaneously perturbed by the interaction. A clear illustration of this is to compare the velocity and pressure gradients for a given shock acceleration, which cannot simultaneously match the gradients in the simple wave. The ratio of the pressure gradient to the velocity gradient in the incident simple wave is

$$\frac{1}{\rho_1 a_1} \frac{P_x}{u_x} = \frac{\rho_2 a_2}{\rho_1 a_1}, \quad (5.1)$$

and the ratio behind a shock is

$$\frac{1}{\rho_1 a_1} \frac{P_{x,2}}{u_{x,2}} = \frac{G}{F}. \quad (5.2)$$

These two quantities are generally not equal. For moderate strength shocks in gases with  $1 \leq \gamma \leq 5/3$ , then

$$\frac{G}{F} \frac{\rho_1 a_1}{\rho_2 a_2} > 1, \quad (5.3)$$

which increases for greater  $M$  and smaller  $\gamma$ . Clearly, both the pressure and velocity gradients behind a decaying shock wave cannot be simultaneously matched to the incident gradients of a simple wave. The wave reflected by the interaction is necessary to match flow gradients with the values given by shock-change equations. The initial gradients are perturbations of the incident values.

The perturbed post-shock state can be modeled as

$$\begin{aligned} u &= u^{(0)} + u^{(1)}, \\ P &= P^{(0)} + P^{(1)}, \end{aligned} \quad (5.4)$$

where superscript (0) terms describe the incident simple wave, and superscript (1) terms describe the perturbation by the reflected wave.  $u$  and  $P$  are the flow variables in the general

region behind the shock. The approximation is that  $u^{(0)} \gg u^{(1)}$  and  $P^{(0)} \gg P^{(1)}$ . Then, to leading order, the  $C^+$  characteristic equation is (Landau & Lifshitz 1987, §104)

$$\left[ \frac{\partial}{\partial t} + (u^{(0)} + a^{(0)}) \frac{\partial}{\partial x} \right] \left( u^{(1)} + \frac{P^{(1)}}{\rho^{(0)} a^{(0)}} \right) = 0, \quad (5.5)$$

and so gradients along  $C^+$  characteristics are given by

$$u_x^{(1)} + \frac{P_x^{(1)}}{\rho^{(0)} a^{(0)}} - \frac{P^{(1)}}{(\rho^{(0)} a^{(0)})^2} \frac{\partial \rho^{(0)} a^{(0)}}{\partial x} = 0. \quad (5.6)$$

When the simple wave initially overtakes the shock, the reflected wave only perturbs the derivatives of post-shock flow variables, so that at the shock

$$\begin{aligned} u_2^{(1)} &= 0, \\ P_2^{(1)} &= 0, \end{aligned} \quad (5.7)$$

and (5.6) becomes

$$u_{x,2}^{(1)} + \frac{P_{x,2}^{(1)}}{\rho_2 a_2} = 0. \quad (5.8)$$

The perturbation (5.4) can be applied to the shock-change equations, giving

$$F \dot{M} = u_{x,2}^{(0)} + u_{x,2}^{(1)}, \quad (5.9)$$

$$\rho_1 a_1 G \dot{M} = P_{x,2}^{(0)} + P_{x,2}^{(1)}. \quad (5.10)$$

From a  $C^-$  characteristic through the simple wave, the unperturbed gradients are related by

$$u_{x,2}^{(0)} - \frac{P_{x,2}^{(0)}}{\rho_2 a_2} = 0. \quad (5.11)$$

Equations (5.8) and (5.11) can be used to eliminate the pressure gradient terms from (5.10), which gives

$$\rho_1 a_1 G \dot{M} = \rho_2 a_2 (u_{x,2}^{(0)} - u_{x,2}^{(1)}), \quad (5.12)$$

and (5.12) can be combined with (5.9) to eliminate the perturbation term,  $u_{x,2}^{(1)}$ . The result is

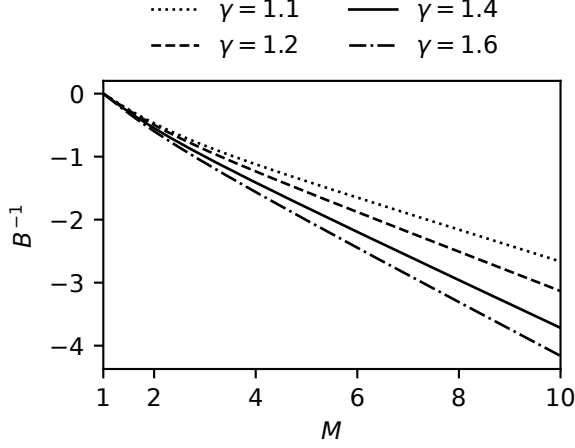
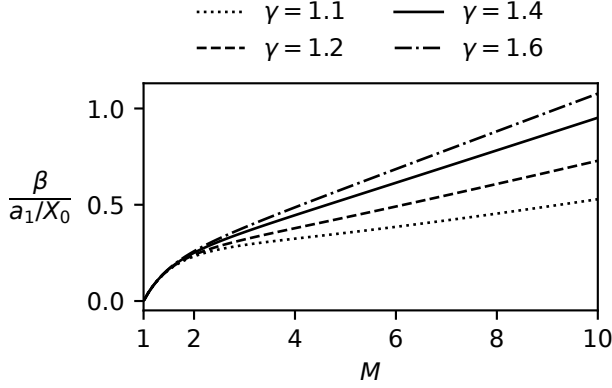
$$\frac{1}{2} \left( F + \frac{\rho_1 a_1}{\rho_2 a_2} G \right) \dot{M} = u_{x,2}^{(0)}. \quad (5.13)$$

For a given simple wave incident upon a shock with initial velocity gradient  $u_{x,2}^{(0)}$ , the shock-change equation (5.13) can be used to compute the initial shock acceleration, where the resulting velocity and pressure gradients are consistent with an acoustic perturbation to the incident simple wave. It is convenient to express (5.13) with a new coefficient,

$$B = \frac{1}{2} \left( F + \frac{\rho_1 a_1}{\rho_2 a_2} G \right), \quad (5.14)$$

the inverse of which is plotted in figure 5 for a perfect gas with various  $\gamma$ .

Equation (5.13) can be used to calculate the initial shock decay rate,  $\beta$ , defined by (4.3). For a centered wave in a perfect gas,  $u_{x,2}^{(0)}$  is given by (2.6), where  $t$  is the time when the wave first intersects the shock. Figure 6 plots  $\beta$  for various  $\gamma$ .

Figure 5:  $B^{-1}$  for a range of  $M$  and  $\gamma$ Figure 6: Variation in  $\beta$  with  $M$  and  $\gamma$ , where  $\beta$  is given by (4.3)

## 6. Numerical simulations

### 6.1. Methods

Numerical simulations were performed using the open-source finite-volume CFD toolbox OpenFOAM-9 (Greenshields 2021) and the solvers implemented in the library blastFoam-5 (Heylmun *et al.* 2021). The equations of motion are solved in conservative form, so that the tracked variables are  $\{\rho, u, e\}$ . Fluxes are interpolated using the scheme by Kurganov *et al.* (2001) and limited using the functions by van Albada *et al.* (1997) and van Leer (1974). Second-order Runge-Kutta time integration was used. Various validation cases are included in the blastFoam library, including the relevant test problem of interacting blast waves from Woodward & Colella (1984).

For simulations of centered expansion waves, the initial condition corresponds with the time when the piston impulsively stops,  $t = 0$ , as described in section 2. At this time, post-shock conditions for  $P$ ,  $T$ , and  $u$  are uniform from the left domain boundary,  $x = 0$ , up to

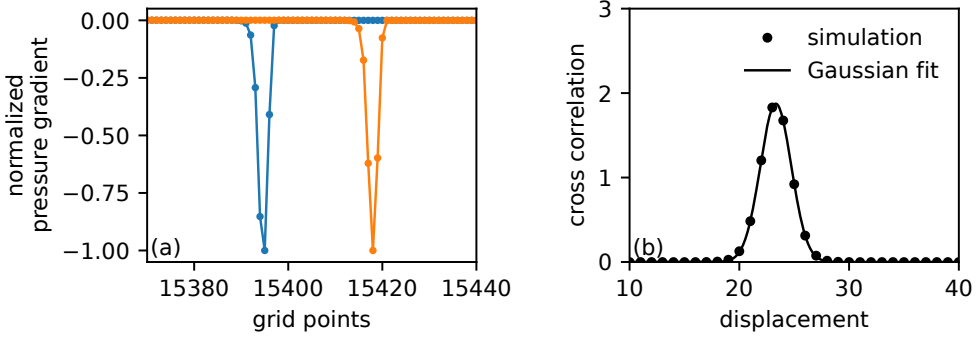


Figure 7: Example of shock displacement calculation using cross correlation of pressure gradients

the shock position at  $x = 1$ . A zero velocity boundary condition at  $x = 0$  causes a centered expansion to form as time advances.

For all simulations, the grid resolution was  $2.5 \cdot 10^3$  cells per unit length, i.e., the initial distance of the shock from the left boundary. Time steps were adjusted to preserve a maximum Courant number of 0.25. Time steps were written to file at a rate adjusted based on the expected initial shock acceleration. The criterion chosen was  $\beta \Delta t = 0.001$ , where  $\Delta t$  is the sampling interval. Simulations were run until shocks had decayed to approximately  $\delta = 0.4$ . The domain lengths were adjusted accordingly. Typical simulation domains were  $5 \cdot 10^4$  cells, and  $3 \cdot 10^3$  time steps written to file. A grid-resolution study including post-processing methods was performed for  $M = 10$  and  $\gamma = 1.4$  for resolutions up to  $10^4$  per unit length and confirmed grid independence of the results.

Shock speeds were measured from simulation results using a cross-correlation algorithm. For every pair of sampled time steps, the cross-correlation of the pressure gradient was computed, and the resulting correlation peak provides an estimate for the shock displacement. Because the numerical shock profile approximates an error function, pressure gradients and their cross correlation are accurately modeled by a Gaussian. Hence, the computed cross-correlations were fit to a Gaussian of the form

$$f(x) = ae^{b(x-x_0)^2}, \quad (6.1)$$

where  $a$ ,  $b$ , and  $x_0$  are fit parameters.  $x_0$  provides a sub-grid-resolution estimate for the shock displacement. This algorithm was chosen for giving much less noisy data than, for example, computing the shock speed from the post-shock pressure or directly differentiating shock position data. Figure 7 illustrates the algorithm. In (a), two pressure gradients are shown, and their cross-correlation is fit to a Gaussian in (b).

In order to quantify residual terms in the second-order shock-change equation (3.34), it was necessary to compute  $\dot{M}$ , which requires numerically differentiating  $M$  twice. This is prone to significant noise, so a smoothing algorithm was employed. Data for  $M$  were smoothed using the Whitaker smoother as described by Eilers (2003). This algorithm was chosen because it does not require interpolation at domain boundaries and so distortion is reduced when compared to other common smoothers. Distortion is nonetheless nonzero, so for estimation of the initial shock acceleration,  $\dot{M}_0$ , a cubic polynomial is fit to the first 100 points of  $M$ , and its derivative is evaluated at the time when the shock begins decaying.

The decay model (4.1) was solved numerically using a fourth-order Runge-Kutta integrator, where  $\dot{M}_0$  was computed using (5.13). For perfect gas calculations,  $K$  is given by (3.43). For

calculations of strong shock waves in equilibrium air,  $K$  is given by (3.35), and all shock-change coefficients were computed using Cantera (Goodwin *et al.* 2021) and the Shock and Detonation Toolbox (Kao *et al.* 2020). This was done by computing the equilibrium post-shock state for a range of shock speeds, and numerically differentiating the resulting data.

Thermodynamics for equilibrium air composed of 21% O<sub>2</sub> and 79% N<sub>2</sub> were computed with Cantera using the ninth-order polynomials given by McBride *et al.* (2002) including ionic species. For implementation of equilibrium air in OpenFOAM, the equation of state was specified using tabular look-up methods available in blastFoam, where  $P$  and  $T$  are given in terms of tabular data of  $\rho$  and  $e$ . The data tables were generated using Cantera.

## 6.2. Decay by a centered expansion in a perfect gas

The time evolution of velocity, pressure, and their gradients is shown in figure 8 for a representative case with  $M_0 = 7$  and  $\gamma = 1.4$ . Artifacts in the gradients at the shock front were eliminated by downsampling the data by a factor of five before computing the gradient. The leftmost contour corresponds to a time just before the expansion wave is incident upon the shock, and subsequent contours are after the shock has begun decaying. The interaction reflects a left-propagating wave along  $C^-$  characteristics, which introduces kinks in the velocity and pressure profiles. Although not obvious from (a) and (c), they are apparent in the velocity and pressure gradients in (b) and (d) as step discontinuities. This discontinuity propagates along the leading characteristic of the reflected wave and in (b) is not to be mistaken for a small numerical artifact that is apparent in early profiles. The pressure gradient in (d) shows a kink between the step discontinuity and the shock front, which corresponds to the particle path that bounds the region of nonuniform entropy. These features in both the velocity and pressure profiles are clearly weak compared with the gradients introduced by the incident centered wave, which is consistent with the claim made in section 5 that they can be modeled as perturbations.

The initial shock acceleration,  $\dot{M}_0$ , was measured from simulation results and compared with the value predicted using three estimates. The relative error of these three estimates is shown in figure 9 for three values of  $\gamma$  and  $M_0$  ranging from 1.5 to 10, where the relative error is given by  $\dot{M}_{0,\text{est}}/\dot{M}_{0,\text{sim}} - 1$ . As discussed in section 5,  $u_{x,2}^{(0)}$  and  $P_{x,2}^{(0)}$  are the velocity and pressure gradients in the incident centered expansion, unperturbed by the reflected wave from the interaction with the shock. Using these quantities and their shock-change equations directly introduces significant error for small  $\gamma$  and large  $M_0$ . The method described in section 5 uses the shock-change coefficient,  $B$ , that takes into account the effect of a weak acoustic perturbation and is effectively an average of the two other methods. The result is that  $u_{x,2}^{(0)}/B$  is a consistently more accurate prediction of  $\dot{M}_0$ . The average error is uniformly 0.5%, and this is attributed in part to the numerical methods.

In figure 10 results from a simulation for  $M_0 = 3$  and  $\gamma = 1.4$  are used to evaluate the accuracy of various theories from prior work including the new model given by (4.1). Solutions by Chandrasekhar (1943), Brinkley & Kirkwood (1947), Friedrichs (1948), Sharma *et al.* (1987), Best (1991), and Sharma & Radha (1994) are plotted. Details on implementation of these theories are described in Appendix A. It is important to note that, except for Friedrichs (1948) and Sharma *et al.* (1987), all theories require the initial shock acceleration to be known, so the solution (5.13) was used for this. Clearly, the present model is most accurate, nearly indistinguishable from the simulation results. Theories by Chandrasekhar (1943) and Brinkley & Kirkwood (1947) are both also quite accurate, and so they are compared with the present model and simulation results for a stronger shock,  $M_0 = 7$ , in figure 11. In this

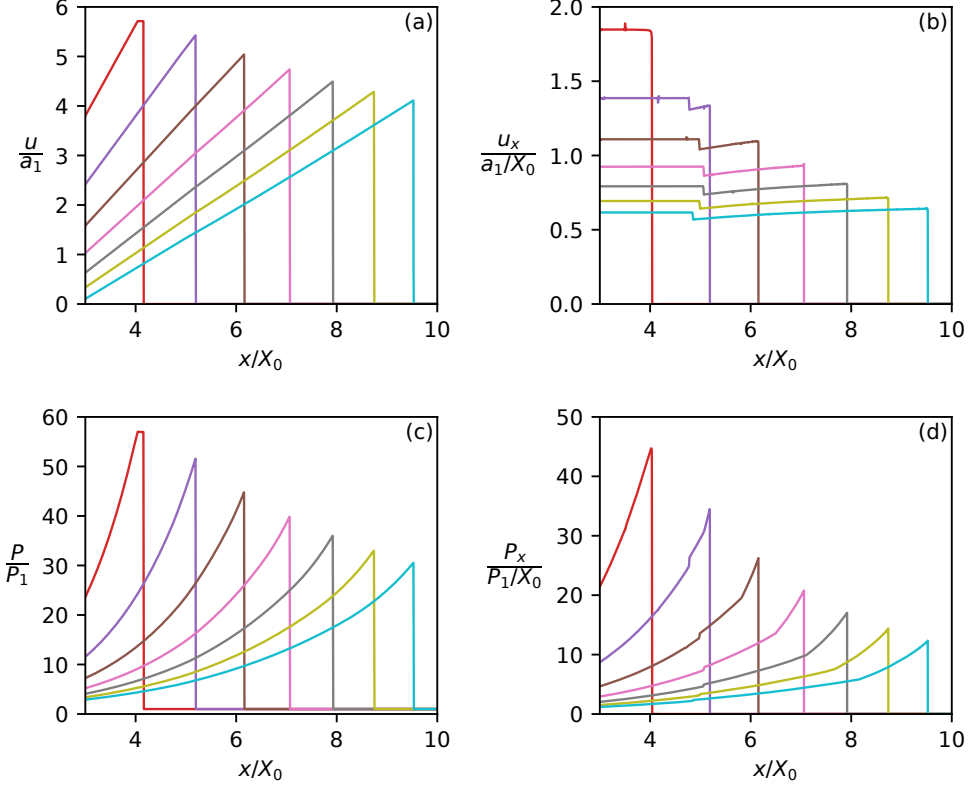


Figure 8: Early evolution of velocity, pressure, and their gradients for  $M_0 = 7$  and  $\gamma = 1.4$ . The leftmost profile corresponds to  $t = 0.381\sqrt{\gamma}$ , just prior to wave incidence, and  $\Delta t = 0.127\sqrt{\gamma}$  between each subsequent profile

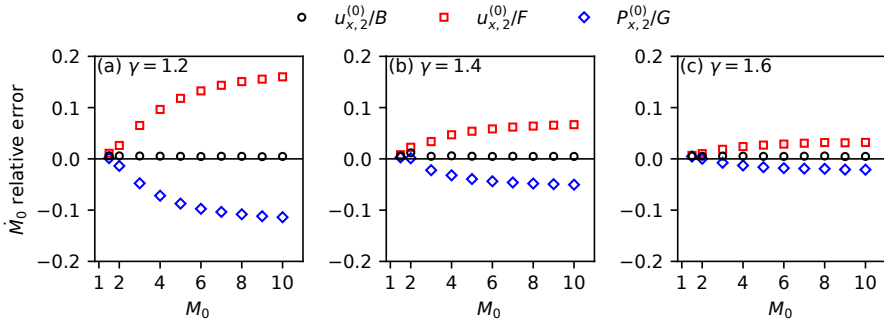


Figure 9: Estimates of  $\tilde{M}_0$  using shock-change equations with unperturbed gradients in incident simple wave compared with values measured from numerical simulations

case, the other models begin to diverge from the simulation results, but the present model still closely agrees.

The present model is compared to three simulation cases in figure 12 with  $M_0 = 3$ ,  $M_0 = 6$ , and  $M_0 = 9$  for  $\gamma = 1.4$ . The time-evolution of the relative error between the model and simulation, given by  $M_{\text{model}}/M_{\text{sim}} - 1$ , is shown in (b). Shock decay is slightly faster for

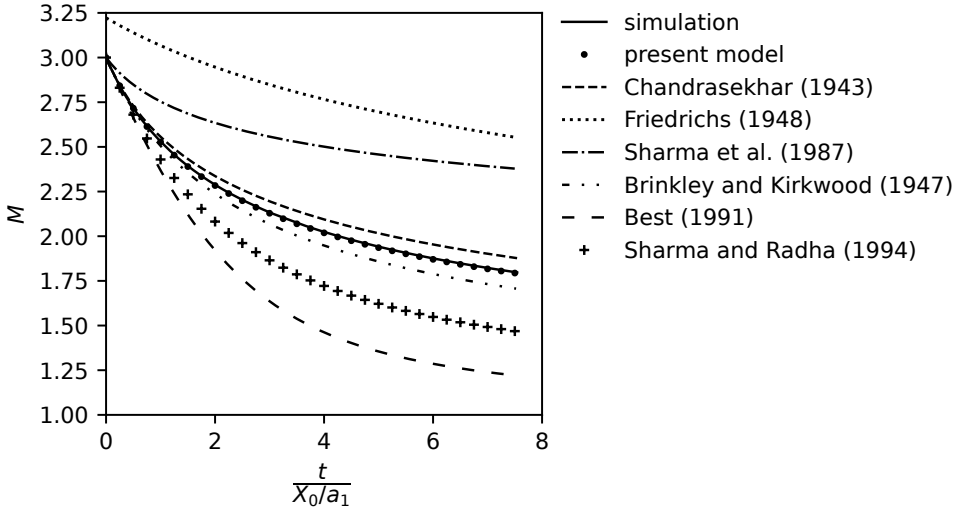


Figure 10: Comparison of various theories for the decay of a  $M_0 = 3$  and  $\gamma = 1.4$  shock with simulation results and our model

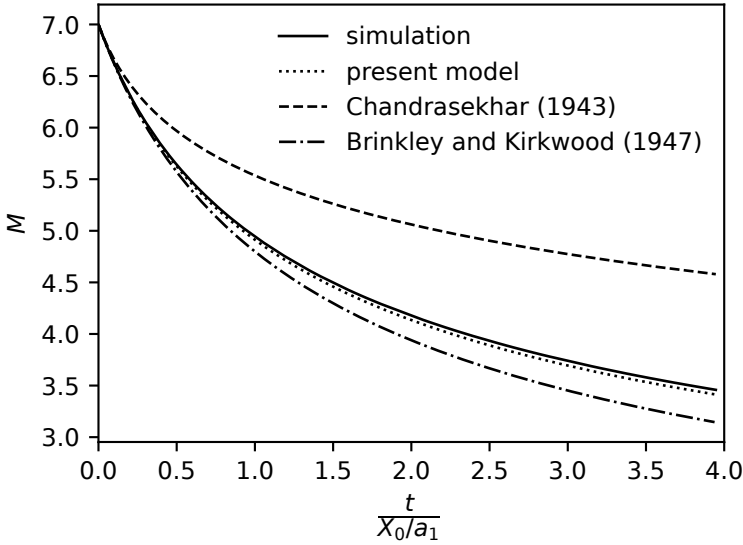


Figure 11: Comparison for the decay of a  $M_0 = 7$  and  $\gamma = 1.4$  shock

the model, such that errors are uniformly negative. For  $M_0 = 3$ , it appears that the error approaches a constant value, but for  $M_0 = 6$  and  $M_0 = 9$  it is still increasing in magnitude. Although the duration in time of each simulation is not the same, they capture the same amount of shock decay,  $\delta = 0.4$ .

Since errors are largest at final simulation time, they are plotted in figure 13 for all simulated cases. The dependence on  $\gamma$  is shown with additional data for  $M_0 = 7$  in (b). Error is larger

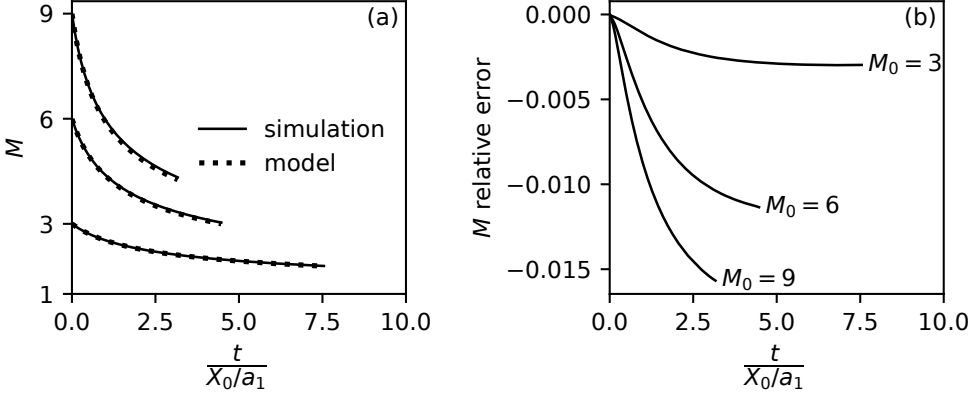


Figure 12: Time-evolution of (a)  $M$  from numerical simulations and model predictions and (b) model error. All cases are for  $\gamma = 1.4$

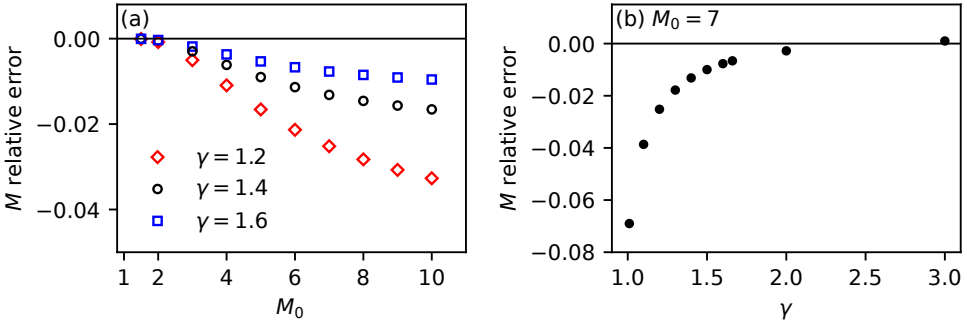


Figure 13: Relative error in model prediction for  $M$  at end of simulated time, corresponding to  $\delta = 0.4$ . Dependence on  $\gamma$  is shown with more data in (b) for  $M_0 = 7$

for smaller  $\gamma$  and increasing  $M_0$ . For shock decay up to  $\delta = 0.4$ , error for  $\gamma = 1.2$  is less than 3%, error for  $\gamma = 1.4$  is less than 2%, and error for  $\gamma = 1.6$  is less than 1%. For  $M_0 = 7$ , error is nearly 7% for  $\gamma = 1.01$ .

Other than the estimate for  $\dot{M}_0$ , the only assumption in the model is that  $u_{xx,2} = 0$ , and so the nonzero errors in figure 13 illustrate that this is not exactly true. Although  $u_{xx,2} = 0$  in the initial centered expansion, the interaction with the shock generates a perturbation to the flow resulting in a nonzero value for  $u_{xx,2}$ . The shock-change equation for  $u_{xx,2}$  (3.34) is analytically exact, and so can be used to compute the magnitude of the perturbation from simulation data. In figure 14, the terms of (3.34) are plotted for the simulation case  $M_0 = 7$  and  $\gamma = 1.4$ , where  $K$  is computed using the simulated  $M$ . In (a),  $\dot{M}$  and  $-K\dot{M}^2$  are nearly indistinguishable. From (3.34), their difference is the residual term  $a_1 L u_{xx,2}$ , which is plotted in (b) and shows a small nonzero value initially, before rapidly decreasing to near zero. The initial magnitude of the terms in (a) is roughly twenty times greater than the initial value in (b), which shows that the perturbation is small compared to the terms in (a) and illustrates why the approximation  $u_{xx,2} = 0$  produces such accurate predictions of the shock propagation.

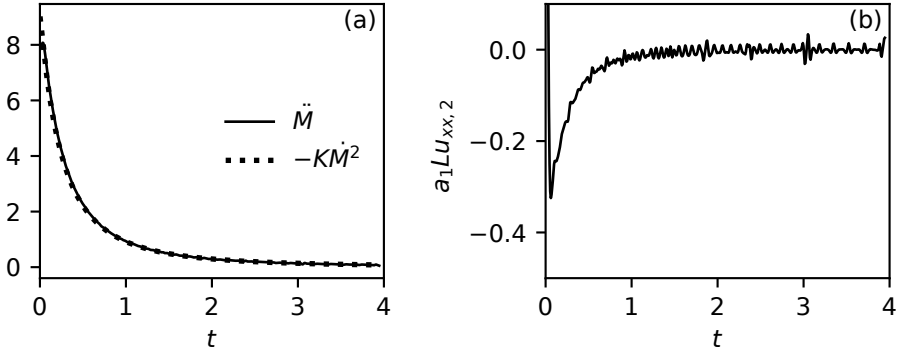


Figure 14: Terms from second-order shock-change equation (3.34) evaluated from simulation data for  $M_0 = 7$   $\gamma = 1.4$ , where quantities are nondimensionalized using time scale  $X_0/a_1$

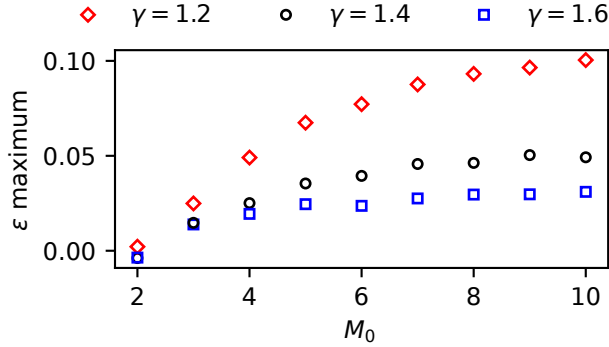


Figure 15: Maximum value of  $\epsilon$ , which quantifies the perturbation by the reflected wave

The exact shock-change equation (3.34) can be reformulated to obtain a small parameter in terms of  $u_{xx,2}$ ,

$$\ddot{M} + K\dot{M}^2 (1 + \epsilon) = 0 \quad (6.2)$$

$$\epsilon = a_1 \frac{Lu_{xx,2}}{K\dot{M}^2}. \quad (6.3)$$

Now, the model  $u_{xx,2} = 0$  can be considered the limit of  $\epsilon \ll 1$ . The maximum value for  $\epsilon$  is at time  $t = 0$  when the perturbation is strongest. This is estimated from simulation data and plotted in figure 15, which shows that  $\epsilon$  is largest for decreasing  $\gamma$  and increasing  $M_0$ , consistent with the errors in figure 13.

In contrast, for the analogous formulations used by Best (1991) and Sharma & Radha (1994), where the equivalent residual term is defined by  $\partial_t(P_t + \rho au_t)$  and  $P_{xx}$ , respectively, the residual term is never small because the gradients are never small in the incident simple

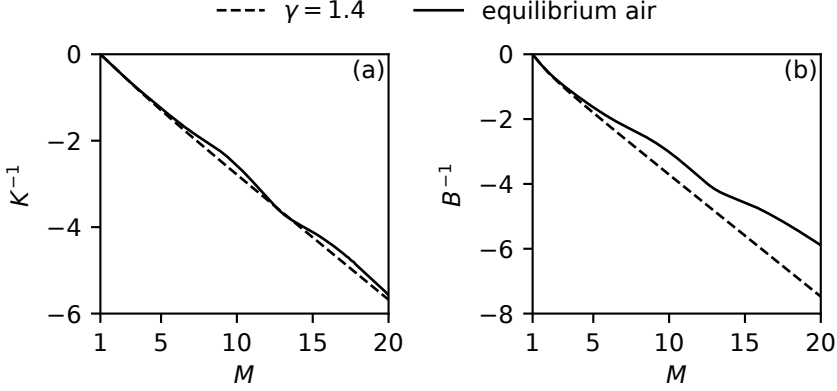


Figure 16: Shock-change coefficients  $K^{-1}$  and  $B^{-1}$  for shock Mach numbers up to 20 in a  $\gamma = 1.4$  gas and in equilibrium air initially at 50 kPa, 300 K air (21%  $O_2$  and 79%  $N_2$ )

wave, regardless of the reflected perturbation. For example, the equation for  $P_{xx,2}$  is

$$\ddot{M} + J\dot{M}^2 (1 + \hat{\epsilon}) = 0 \quad (6.4)$$

$$\hat{\epsilon} = \frac{NF^2}{J} \frac{P_{xx,2}}{\rho_1 u_{x,2}^2}. \quad (6.5)$$

In a centered expansion in a perfect gas,  $P_{xx,2}$  at the head of the wave is given by

$$\frac{P_{xx,2}}{\rho_1} = \frac{\gamma + 1}{2} \frac{\rho_2}{\rho_1} u_{x,2}^2. \quad (6.6)$$

Neglecting the perturbation by the reflected wave, then for  $\gamma = 7/5$  and  $M = 5$ ,  $\hat{\epsilon} = 5.37$ , whereas for the  $u_{xx,2}$  formulation  $\epsilon = 0$ , exactly.

### 6.3. Decay by a centered expansion in equilibrium air

Figure 16 shows calculations of the shock-change coefficients relevant to the decay model,  $K$  and  $B$ , for  $M$  up to 20. In (a)  $K^{-1}$  remains roughly linear. In (b),  $B^{-1}$  diverges significantly from  $\gamma = 1.4$ , indicating that for a given  $u_x^{(0)}$ , the initial shock decay rate is greater in equilibrium air.

Simulations were performed for three shock Mach numbers (5, 10, and 15) in air initially at 50 kPa and 300 K. In figure 17(a), the shock Hugoniot and isentrope are plotted. Also shown is the chemically frozen Hugoniot. Figure 17(b) shows the tabular data for  $P(\rho, e)$ , where  $P$  is normalized by the chemically frozen pressure,  $P_{fr}$ , at the same  $\rho$  and  $e$ . The shock Hugoniot and isentropes are also plotted in figure 17(b), where the area bounded by the curves contains all thermodynamic states accessed by the simulated flow.

Results from numerical simulations are compared with model predictions in figure 18. The time-evolution of the shock Mach number is shown in (a), (b), and (c), and the relative error is shown in (d). The model accuracy is excellent with error less than 1% for both  $M_0 = 5$  and  $M_0 = 10$  cases and less than 2% for  $M_0 = 15$ . This clearly shows that the model is effective even for equations of state very different from a perfect gas. Results for  $\gamma = 1.4$  are also shown for comparison. The large error can be attributed to the discrepancy in  $B^{-1}$  shown in 16(b).

The power-law approximation can also be applied for problems with general equations of

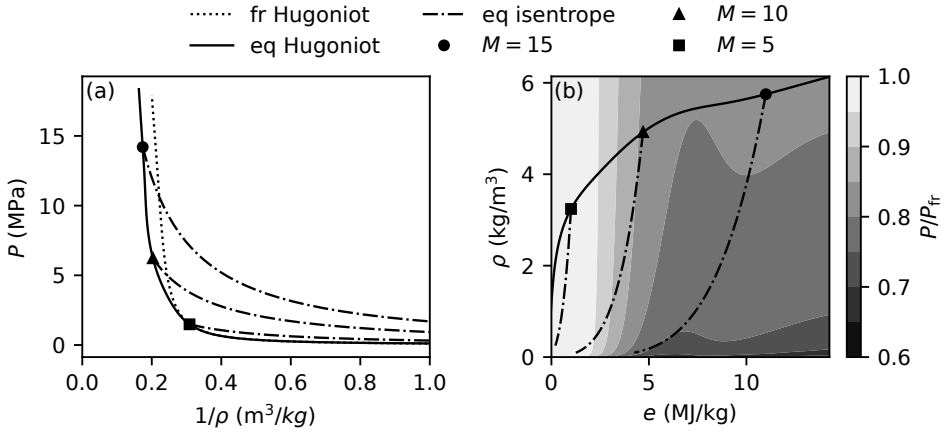


Figure 17: Thermodynamics for simulations of shocks in equilibrium air. (a) shock Hugoniot and isentropes, (b) contours of tabular data for  $P = P(\rho, e)$ . Abbreviations “fr” and “eq” denote chemically frozen and equilibrium, respectively

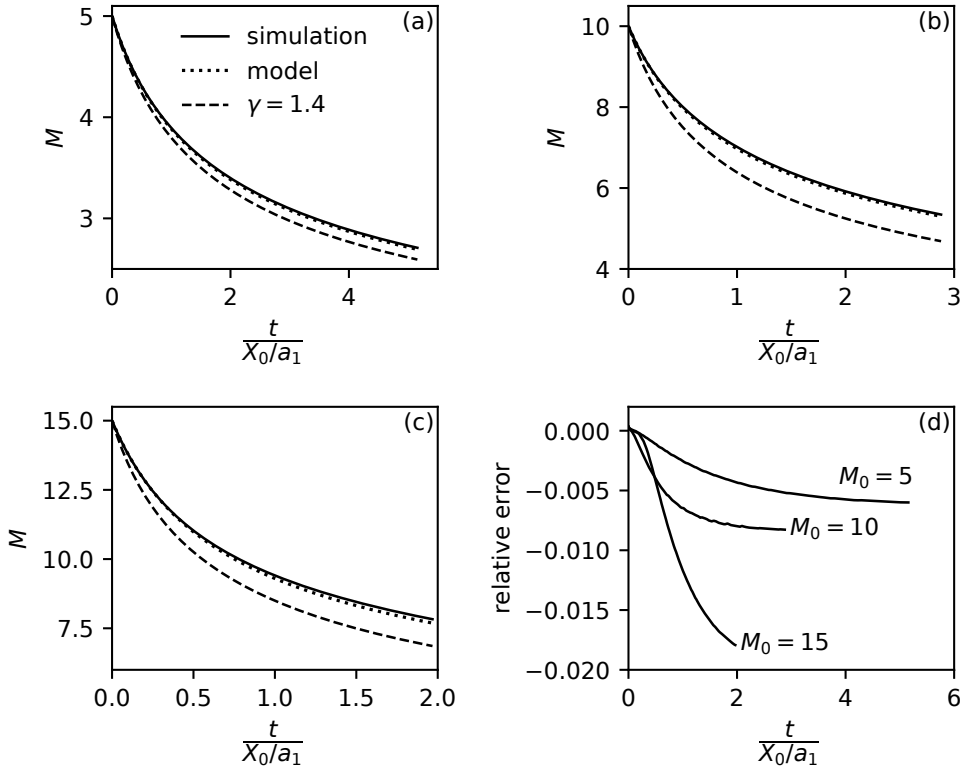


Figure 18: Comparison between numerical simulations and model predictions for strong shocks in equilibrium air initially at 50 kPa and 300 K

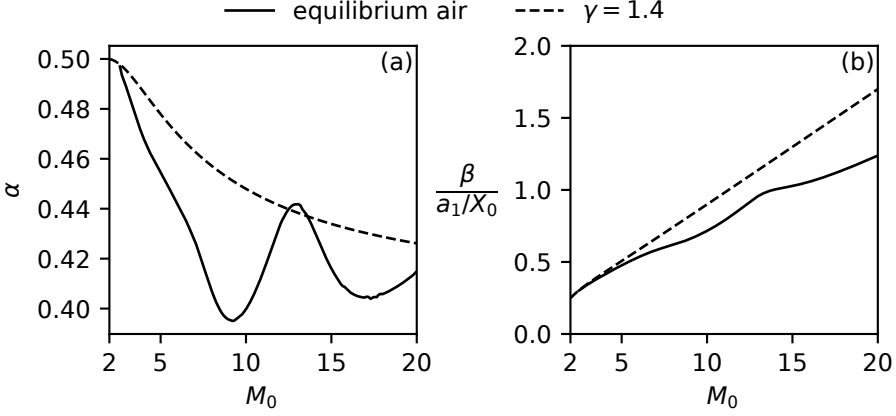


Figure 19: Parameters for power-law approximation of decay model for equilibrium air at 50 kPa and 300 K

state, where  $K(M_0)$  is computed accordingly. Figure 19 shows  $\alpha$  and  $\beta$  for  $M$  up to 20. The non-monotonic behavior of  $\alpha$  as  $M_0$  increases is due to the sequential effects of vibrational excitation, chemical dissociation, and ionization in equilibrium air. Similar behavior can be observed from plots of  $\gamma$  (Henderson & Menart 2008).

The interaction with the centered wave for equilibrium air did not introduce a larger perturbation to the incoming simple wave than for a perfect gas. As discussed in 2, the other source for nonzero  $u_{xx,2}$  is in variation of  $\Gamma$  on  $C^+$  characteristics in the simple wave.  $\Gamma$  and  $a_1 \partial_a \Gamma$  are plotted in figure 20 along the post-shock isentrope of the  $M_0 = 15$  case. These values can be used with (3.34) to estimate the maximum  $\epsilon$ , where  $\epsilon$  is given by

$$\begin{aligned} \epsilon &= a_1 \frac{L u_{xx,2}}{K M^2}, \\ &= -a_1 \frac{L F^2}{K} \frac{\Gamma - 1}{\Gamma} \partial_a \Gamma. \end{aligned} \quad (6.7)$$

For  $M_0 = 15$ ,  $LF^2/K = 2.16$ . Then, using the maximum values shown in figure 20 for  $\Gamma$  and  $a_1 \partial_a \Gamma$  gives  $\epsilon \leq .014$ . So, for equilibrium air at these conditions, the effect of nonconstant  $\Gamma$  is negligible, and the model assumption that  $u_{xx,2} \approx 0$  holds.

#### 6.4. Decay by a simple wave from the constant deceleration of a piston in a perfect gas

If the piston does not impulsively stop, but instead slows at a gradual rate, then a non-self-similar simple wave is generated. If the piston slows with a constant acceleration to a halt, then the piston velocity,  $v$ , and position,  $X_p$ , over time are given by the piecewise expressions

$$v = \begin{cases} u_2(1 - t/\tau_s) & 0 \leq t \leq \tau_s, \\ 0 & t \geq \tau_s \end{cases}, \quad X_p = \begin{cases} u_2 t \left(1 - \frac{t}{2\tau_s}\right) & 0 \leq t \leq \tau_s, \\ \frac{u_2 \tau_s}{2} & t \geq \tau_s \end{cases}, \quad (6.8)$$

where  $\tau_s$  is the time when the piston is fully stopped. The solution for the simple wave is given by (2.2), where  $f(u)$  is obtained from the piston path. The procedure is demonstrated for an exponential piston by Zel'dovich & Raizer (1967), however in that case the result is implicit. For a constant-deceleration piston, all quantities can be found explicitly throughout

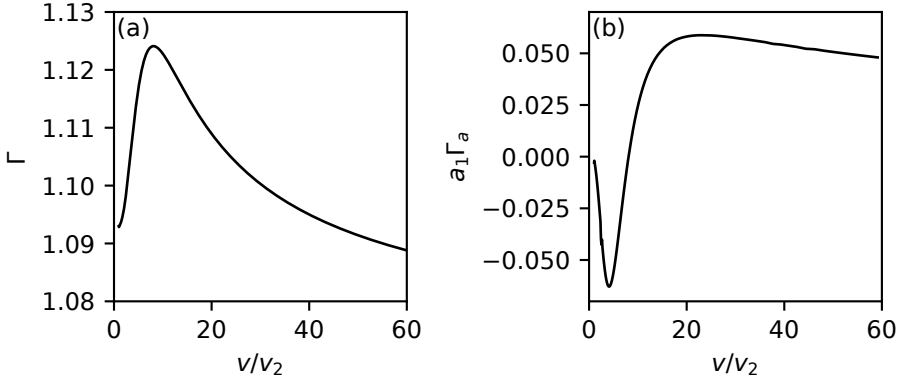


Figure 20: Variation of (a)  $\Gamma$  and (b)  $a_1 \partial_a \Gamma$  along  $M_0 = 15$  post-shock isentrope, where  $v_2$  is the post-shock specific volume

the wave. At the piston face,  $u = v$  and so

$$f(v) = X(t(v)) - (v + a(v))t(v), \quad (6.9)$$

where time is expressed in terms of the piston speed, i.e.,  $t = \tau_s(1 - v/u_2)$ . For a perfect gas, the sound speed is given by

$$a(u) = \frac{\gamma - 1}{2}(u - u_2) + a_2, \quad (6.10)$$

and so (6.9) can be simplified to obtain the general expression for  $f(u)$  in the simple wave,

$$f(u) = \frac{u_2 \tau_s}{2} \left( 1 - \left( \frac{u}{u_2} \right)^2 \right) - \left[ \frac{\gamma + 1}{2}u - \frac{\gamma - 1}{2}u_2 + a_2 \right] \left( 1 - \frac{u}{u_2} \right) \tau_s. \quad (6.11)$$

With  $f(u)$ ,  $u(x, t)$  throughout the simple wave can be obtained from (2.2),

$$\begin{aligned} \frac{u}{u_2} = 1 - \frac{a_2}{\gamma u_2} - \frac{\gamma + 1}{2\gamma} \frac{t}{\tau_s} \\ + \frac{1}{\gamma} \sqrt{\left( \frac{\gamma + 1}{2} \frac{t}{\tau_s} \right)^2 + 2\gamma \left( \frac{x}{u_2 \tau_s} - \frac{t}{\tau_s} \right) - (\gamma - 1) \frac{a_2}{u_2} \frac{t}{\tau_s} + \left( \frac{a_2}{u_2} \right)^2}. \end{aligned} \quad (6.12)$$

The sound speed can be obtained from (6.10), and other quantities follow from isentropic relations.

The velocity gradients,  $u_x$  and  $u_{xx}$ , are found by differentiating (6.12). The result for  $u_{xx}$  can be simply expressed as

$$u_2 u_{xx} = -\gamma \tau_s u_x^3, \quad (6.13)$$

which is valid throughout the wave.

With the additional time scale,  $\tau_s$ , a single additional nondimensional variable distinguishes resulting shock motions given by  $\sigma = \tau_s/\tau_p$ , where  $\tau_p$  is the duration of the constant velocity phase of the piston motion. For  $\sigma \rightarrow 0$ , a centered expansion wave is obtained. For  $\sigma \rightarrow \infty$ , there is no initial steady phase of the piston motion, and the shock is formed decaying at the

piston face. In this limit, the maximum value for  $u_{xx}$  at the shock is at  $t = 0$  and given by

$$\frac{a_1 u_{xx,2}}{u_{x,2}^2} = -\gamma \frac{a_1}{a_2}, \quad (6.14)$$

which can be used to estimate  $\epsilon$  from the exact shock-change equation and is equal to

$$\epsilon = -\gamma \frac{LF^2}{K} \frac{a_1}{a_2}. \quad (6.15)$$

For  $M_0 = 7$  and  $\gamma = 1.4$ ,  $\epsilon = -0.61$ , which is clearly not small and shows that the general piston motion introduces a significant deviation from the  $u_{xx,2} = 0$  model.

For decreasing  $\sigma$ , there is more time for the simple wave to approach the linear-velocity profile of a centered expansion, and so the  $u_{xx,2} = 0$  model accuracy is expected to increase. For larger  $\sigma$ , where  $u_{xx,2}$  is non-negligible, we can still use the value in the unperturbed wave and neglect the disturbance by reflected waves. In this case, (6.13) is used in the shock-change equation (3.34). Instead of directly computing the velocity gradient, it is estimated using its shock-change equation and the value for the shock acceleration.  $u_{xx,2}$  is then approximated by

$$u_{xx,2} = -\gamma \tau_s (F\dot{M})^3 / u_2, \quad (6.16)$$

which enables (3.34) to be solved as a second-order initial value problem. The initial shock acceleration is still given by (5.13), where the velocity gradient at the head of the unperturbed wave is

$$u_{x,2}^{(0)} = \left[ \frac{\gamma + 1}{2} t_0 + \frac{a_2}{u_2} \tau_s \right]^{-1}. \quad (6.17)$$

In order to numerically simulate the shock decay by these simple waves, three cases for a shock with  $M_0 = 7$  and  $\gamma = 1.4$  were considered with values of  $\sigma = 0.25$ ,  $\sigma = 0.5$ , and  $\sigma = 1.0$ . The simulation was initialized using data computed from the above formulae. For all cases, the initial condition was chosen for a time before the wave is incident upon the shock. The initial conditions are shown in figure 21. For  $\sigma = 0.5$  and  $\sigma = 0.25$ , the piston velocity is not zero at the beginning of the simulation. For these cases, the left boundary condition is set to the constant piston velocity at the beginning of the simulation, so that the piston is no longer slowing. Characteristics from the wall do not reach the shock within simulation time.

Results from numerical simulations are plotted with the model prediction in figure 22. Subplots (a), (b), and (c) show that, as expected, as  $\sigma$  increases the agreement with the  $u_{xx,2} = 0$  model decreases. Accordingly, subplots (d), (e), and (f) show that the error increases. Also plotted in figure 22 are the model results from using the unperturbed value of  $u_{xx,2}$  in the incident simple wave, which was approximated using (6.16). This achieves less than 2% error for all cases, which is similar to the error in section 6.2 for  $M_0 = 7$  and  $\gamma = 1.4$ . These results show that even for non-self-similar simple waves, the shock-propagation model obtained by neglecting only perturbations to the incident second velocity gradient remains accurate.

## 7. Summary and conclusions

A model for the decay of plane shock waves in equilibrium flows with an arbitrary equation of state was formulated using a shock-change equation for the second velocity gradient behind the shock,  $u_{xx}$ . In contrast to prior work, instead of neglecting all higher-order gradients, only the perturbation to those gradients by the shock interaction is neglected.

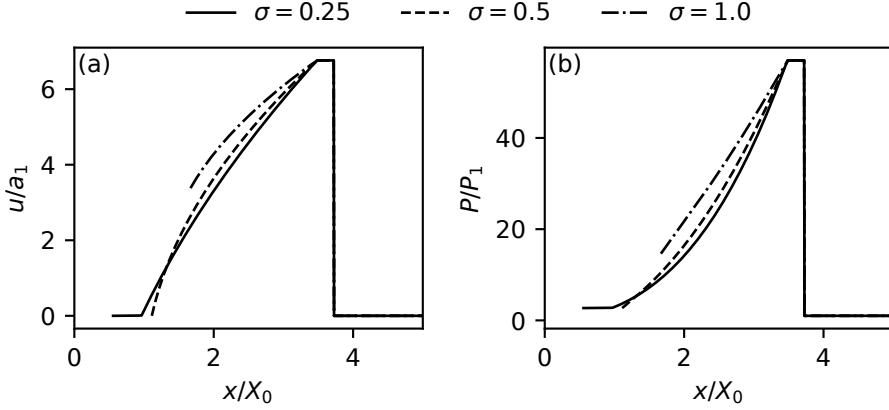


Figure 21: Initial (a) particle velocity and (b) pressure for simulations of shock decay by the simple wave from a constant-deceleration piston for  $M_0 = 7$  and  $\gamma = 1.4$

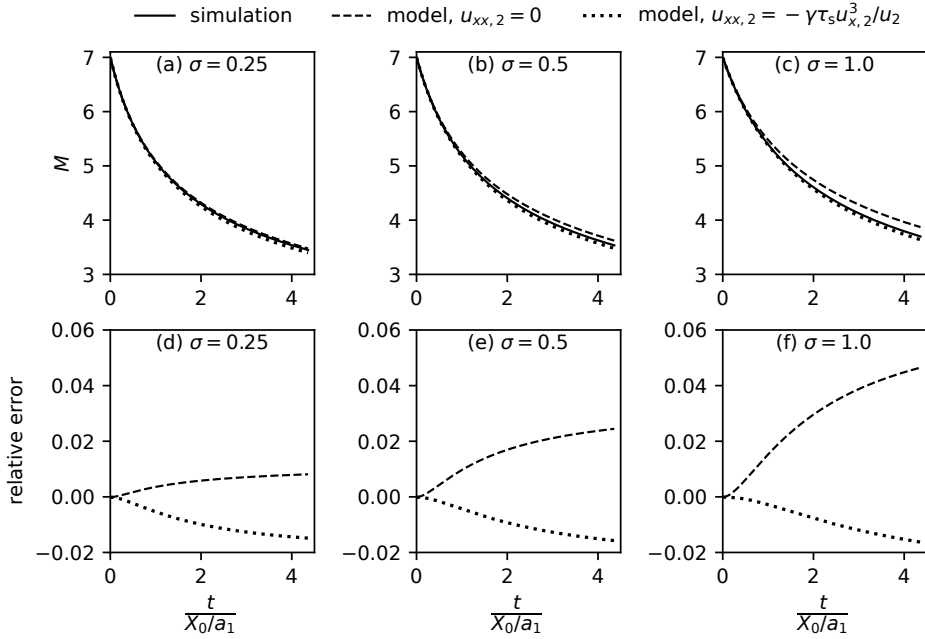


Figure 22: Time evolution of (a,b,c) shock speed and (d,e,f) model error for  $M_0 = 7$  and  $\gamma = 1.4$  shocks decayed by the simple wave from a constant-deceleration piston for three values of the scale parameter,  $\sigma$

For centered expansion waves in a perfect gas,  $u_{xx} = 0$  exactly throughout the wave, and therefore also behind a decaying shock if the perturbation is neglected. Comparison with numerical simulations showed that these perturbations are indeed sufficiently small to obtain accurate solutions for the shock trajectory. For a general equation of state,  $u_{xx} \neq 0$  in the incident simple wave due to variation in the fundamental derivative of gas dynamics,  $\Gamma$ . For a centered wave in equilibrium air, it was shown that this variation is small, and  $u_{xx} = 0$  remains an accurate model even for a Mach 15 shock. For an arbitrary simple wave,  $u_{xx} \neq 0$

and must be accounted for. This can still be accomplished by neglecting the perturbation from the shock interaction, which was shown to be effective for the simple wave generated by the constant deceleration of a piston in a perfect gas. Since simple waves converge to a self-similar solution, then in some cases  $u_{xx} = 0$  can still be used for arbitrary simple waves and remains a good initial estimate.

The value of the analytical results obtained in this article is in their generality and simple formulation. The model can be readily implemented through numerical solution of a simple ordinary differential equation (4.1), where  $K$  is given for an arbitrary equation of state in (3.35) and for a perfect gas in (3.43). The initial shock acceleration can be computed from (5.13), where  $u_{x,2}^{(0)}$  is the velocity gradient in the incident simple wave, which is given by (2.5). A useful result from this analysis is an approximate power-law formulation, which remains accurate even for cases with strong shocks in equilibrium air. Although not detailed in this article, the model can be used for shocks in media with irreversible endothermic or exothermic reactions, such as overdriven detonation waves. An example of this is described in Appendix C.

Future work might extend the methods to problems with nonplanar shocks, where geometric effects are important. The effectiveness of shock-change models might be evaluated similarly in these cases, where the magnitude of terms are estimated from the unperturbed incident simple waves.

**Funding.** This work was sponsored by the Office of Naval Research (ONR), under grant number N00014-22-1-2141. The views and conclusions contained herein are those of the authors only and should not be interpreted as representing those of ONR, the U.S. Navy or the U.S. Government.

**Declaration of interests.** The authors report no conflict of interest.

**Author ORCIDs.** D. T. Schoeffler, <https://orcid.org/0000-0002-1932-5986>; J. E. Shepherd, <https://orcid.org/0000-0003-3181-9310>

## Appendix A. Implementation of prior theories

### A.1. Chandrasekhar (1943)

Chandrasekhar's solution is given by equation (31) of his work, reproduced here as

$$\frac{M}{(M-1)^2} \frac{(M_0-1)^2}{M_0} e^{M_0-M} = 1 + qt$$

where  $q$  is a required time scale. If  $\dot{M}_0$  is known,  $q$  can be obtained from

$$q = - \left( 1 + \frac{1}{M_0^2} \right) \frac{M_0}{M_0-1} \dot{M}_0.$$

### A.2. Brinkley and Kirkwood (1947)

Brinkley & Kirkwood (1947) derive a propagation equation for one-dimensional shocks in a medium with an arbitrary equation of state. The derivation is based on the equivalence between the work done by some generating surface, e.g., the piston motion, and the residual enthalpy in shocked gas after having isentropically expanded back to the initial pressure,  $P_1$ . The enthalpy increment is nonzero because of the entropy increment by the shock. Lee (2016) discusses this theory in more detail. The Brinkley-Kirkwood shock propagation equations are given by (14) in their work, which were integrated here as they are given. The second-order shock propagation equation requires two initial conditions, given by the shock speed or strength and the blast energy or, equivalently, the initial shock acceleration. The

shock acceleration was computed using this article's solution (5.13) and converted to their variables to give

$$\begin{aligned}\frac{dp}{dR} &= \frac{\partial p}{\partial R} + \frac{1}{U} \frac{\partial p}{\partial t} \\ &= \rho_1 a_1 (G + \hat{G}/M) \dot{M}\end{aligned}$$

where  $R$  is the shock position,  $p$  is the pressure increment at the shock, and  $\hat{G}$  is given in section A.5.

The critical assumption in Brinkley-Kirkwood theory is that the time-evolution of the shock-energy integrand is spatially similar. As a result, the integral over scaled time gives a constant parameter,  $\nu$ . Brinkley and Kirkwood assume the shock-energy time integrand to be exponential and show that a strong shock limit gives  $\nu = 1$  and a weak shock limit gives  $\nu = 2/3$ . For the calculations used in this article,  $\nu = 1$  was used. This was found to be more accurate than  $\nu = 2/3$ . Accuracy was improved for  $\nu > 1$ , but further discussion of this is beyond the scope of the present work.

### A.3. Friedrichs (1948)

Friedrichs's solution for the shock position as a function of time is given by equation (10.13) of his paper. Reproduced here using our nomenclature, the equation is

$$x_s = x_R + a_1 \left[ t - t_R + \frac{4k((t_1 - t_R)(t - t_R))^{1/2}}{1 + k \left( \frac{t_1 - t_R}{t - t_R} \right)^{1/2}} \right], \quad (\text{A } 1)$$

where

$$k = \frac{u_2}{4(1 - \mu^2)a_1 - u_2}$$

and

$$\mu^2 = \frac{\gamma - 1}{\gamma + 1}.$$

$t_R$  and  $x_R$  are the time and position where the piston impulsively stops.  $t_1$  is the time when the head characteristic intersects the shock wave. Friedrichs uses the weak shock approximation, so  $t_1$  is given by

$$t_1 = 8t_R \frac{1 + \mu^2 \sigma_1}{\sigma_1(4 - \sigma_1)},$$

where

$$\sigma_1 = \frac{u_2}{(1 - \mu^2)a_1}.$$

To obtain the shock speed over time, we differentiated (A 1), using the value of  $u_2$  given by the shock jump equations for  $M_0$ . The characteristic time  $t_R$  was scaled to match our time scale.

### A.4. Sharma *et al.* (1987)

The shock propagation equation obtained by Sharma *et al.* (1987) is given by equation (38) of their work. To ensure correct implementation of their solution, it was verified that Figure 2 and Figure 3(b) from their work could be reproduced. Peace & Lu (2018) also implemented this solution, and it was verified that their Figure 4 could be reproduced.

### A.5. Best (1991)

Best (1991) uses a truncation term of the form

$$Q_2 = \frac{1}{\rho_1 a_1^2} \frac{\partial}{\partial t} \left( \frac{\partial P}{\partial t} + \rho a \frac{\partial u}{\partial t} \right) \quad (\text{A } 2)$$

as a generalization of Whitham's geometric shock dynamics. For constant area shock propagation, Best's hierarchy of shock-change equations can be reduced to a single equation in the same form as above. We consider the second-order equation and compare it with our  $u_{xx,2}$  result (3.34). The algebra is simplified by manipulating the equations in terms of the coefficients derived in section 3.

Expanding (A 2) gives

$$Q_2 = \frac{P_{tt,2}}{\rho_1 a_1^2} + \frac{\rho_2 a_2}{\rho_1 a_1} \frac{u_{tt,2}}{a_1} + \frac{\rho_2}{\rho_1} \frac{a_{t,2}}{a_1} \frac{u_{t,2}}{a_1} + \frac{\rho_{t,2}}{\rho_1} \frac{a_2}{a_1} \frac{u_{t,2}}{a_1}. \quad (\text{A } 3)$$

The partial-time shock-change equations are given by

$$\left. \frac{1}{a_1} \frac{\partial u}{\partial t} \right|_2 = \hat{F} \dot{M}, \quad \left. \frac{1}{\rho_1 a_1^2} \frac{\partial P}{\partial t} \right|_2 = \hat{G} \dot{M}, \quad \left. \frac{1}{\rho_1} \frac{\partial \rho}{\partial t} \right|_2 = \hat{H} \dot{M}, \quad \left. \frac{1}{a_1} \frac{\partial a}{\partial t} \right|_2 = \hat{E} \dot{M}, \quad (\text{A } 4)$$

where the coefficients are given by

$$\begin{aligned} \hat{F} &= \frac{\partial u_2}{\partial w_1} - MF, & \hat{G} &= \frac{1}{\rho_1 a_1} \frac{\partial P_2}{\partial w_1} - MG, \\ \hat{H} &= \frac{a_1}{\rho_1} \frac{\partial \rho_2}{\partial w_1} - MH, & \hat{E} &= \frac{\partial a_2}{\partial w_1} - ME. \end{aligned}$$

The second-order shock-change equation for  $u_{tt,2}$  is

$$\begin{aligned} \frac{u_{tt,2}}{a_1} &= \frac{1}{a_1} \frac{du_t}{dt} - M u_{xt,2} \\ &= \frac{1}{a_1} \frac{du_t}{dt} - M \left( \frac{du_x}{dt} - M a_1 u_{xx,2} \right) \\ &= \hat{F}' \dot{M}^2 + \hat{F} \ddot{M} - M F' \dot{M}^2 - M F \ddot{M} - M^2 (\ddot{M} + K \dot{M}^2) / L \\ &= (\hat{F} - M F - M^2 / L) \ddot{M} + (\hat{F}' - M F' - M^2 K / L) \dot{M}^2. \end{aligned} \quad (\text{A } 5)$$

The result for  $P_{tt,2}$  is derived similarly.

Substituting into (A 3) and grouping terms gives the second-order shock-change equation for  $Q_2$ ,

$$\begin{aligned} Q_2 &= \left( \hat{G} - M G - M^2 / N + \frac{\rho_2 a_2}{\rho_1 a_1} (\hat{F} - M F - M^2 / L) \right) \ddot{M} \\ &\quad + \left( \hat{G}' - M G' - J M^2 / N + \frac{\rho_2 a_2}{\rho_1 a_1} (\hat{F}' - M F' - K M^2 / L) + \frac{\rho_2}{\rho_1} \hat{E} \hat{F} + \frac{a_2}{a_1} \hat{H} \hat{F} \right) \dot{M}^2. \end{aligned} \quad (\text{A } 6)$$

Best's theory is to assume  $Q_2 = 0$ , which can be used to solve (A 6) with appropriate initial conditions.

### A.6. Sharma and Radha (1994)

Sharma & Radha (1994) use a series expansion in terms of  $\partial_x^n P$ , where truncation at order  $n$

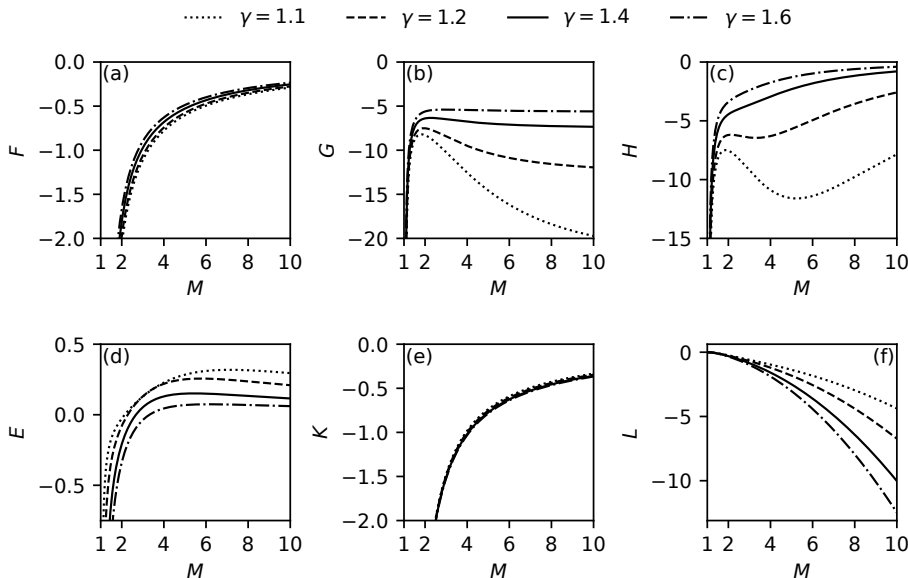


Figure 23: Shock-change coefficients in a perfect gas for a range of  $M$  and  $\gamma$

is used to close the hierarchy of shock-change equations. The required second-order shock-change equation is given by (3.37) and is reproduced here as

$$\ddot{M} + J\dot{M}^2 + N\frac{P_{xx,2}}{\rho_1} = 0.$$

The coefficients,  $J$  and  $N$ , are given by (3.38) and (3.39). The truncation at second order then gives  $P_{xx,2} = 0$ , which reduces (3.37) to a second-order ordinary differential equation requiring the initial conditions  $M_0$  and  $\dot{M}_0$ . The latter is provided by our solution (5.13).

## Appendix B. Shock-change coefficients

Using the formulae from Section 3, figure 23 plots the shock-change coefficients for varying  $M$  and  $\gamma$ . Except for  $E$ , all of the coefficients are uniformly negative.  $E$  crosses zero for some value of  $M$  and  $\gamma$ , which means that when a shock decays through this Mach number, the sound speed gradient changes sign from negative to positive. Except for  $L$ , all of the coefficients exhibit an inverse dependence on  $M$ , tending toward negative infinity as  $M \rightarrow 1$ . This is, of course, partially a consequence of how the coefficients have been defined. They could have instead been defined so that their product with the a flow gradient gives the shock acceleration.

## Appendix C. Irreversible chemical reaction

The shock decay model can also be applied if there is some nonzero heat of reaction,  $\Delta h$ , where  $\Delta h > 0$  is exothermic and  $\Delta h < 0$  is endothermic. If  $\gamma_2 = \gamma_1 = \gamma$ , and  $Q = \Delta h/RT_1$ ,

then the shock jump relations are

$$\frac{P_2}{P_1} = \frac{1 + \gamma M^2}{1 + \gamma M_2^2} \quad (\text{C } 1)$$

$$\frac{v_2}{v_1} = \frac{P_2}{P_1} \frac{M_2^2}{M^2} \quad (\text{C } 2)$$

$$M_2^2 = \frac{-2\gamma\zeta + 1 - \sqrt{1 - 2(\gamma + 1)\zeta}}{(2\gamma\zeta - 1)\gamma + 1} \quad (\text{C } 3)$$

$$\zeta = \frac{M^2}{(1 + \gamma M^2)^2} \left[ \frac{\gamma - 1}{\gamma} Q + 1 + \frac{\gamma - 1}{2} M^2 \right] \quad (\text{C } 4)$$

where  $M_2 = w_2/a_2$ . If  $Q > 0$ , then  $M > M_{\text{CJ}}$ , where  $M_{\text{CJ}}$  is the Chapman-Jouguet (CJ) Mach number, given by

$$M_{\text{CJ}} = \sqrt{\frac{\gamma^2 - 1}{2\gamma} Q + 1} + \sqrt{\frac{\gamma^2 - 1}{2\gamma} Q}. \quad (\text{C } 5)$$

If  $M \geq 1$ , then admissible values for  $Q$  are

$$Q \geq -\frac{\gamma}{2} \frac{\gamma + 1}{\gamma - 1}. \quad (\text{C } 6)$$

Thompson (1972) discusses this model for CJ detonations. The above equations can be used to compute  $K$  and  $B$  for implementation of the decay model.

Figure 24 shows the effect of  $Q$  on  $K^{-1}$  for  $\gamma = 1.2$ . Positive  $Q$  shifts the  $K^{-1}$  to the right, so that  $K^{-1} = 0$  when  $M > 1$ . The value of  $M$  when  $K^{-1} = 0$  is equal to the CJ Mach number. Therefore, the overdriven detonation decays toward the CJ Mach number and approaches it asymptotically with infinite time. Negative  $Q$  results in faster decay for a given shock Mach number. As  $M \rightarrow 1$ ,  $K^{-1}$  remains nonzero and approaches a finite value. As a result, the decaying shock in an endothermic gas approaches  $M = 1$  in finite time. Even small endothermicity results in significant increase in decay as  $M \rightarrow 1$ . These effects are shown by numerical solutions of the shock decay model in figure 25.

For  $Q > 0$ , the power-law approximation can be formulated as

$$\delta(t) = \frac{1}{(1 + \beta t/\alpha)^\alpha}, \quad (\text{C } 7)$$

$$\delta(t) = \frac{M(t) - M_{\text{CJ}}}{M_0 - M_{\text{CJ}}}, \quad \beta = \frac{-\dot{M}_0}{M_0 - M_{\text{CJ}}}, \quad \alpha = -\frac{1}{K(M_0)(M_0 - M_{\text{CJ}}) + 1}.$$

## REFERENCES

- VAN ALBADA, G. D., VAN LEER, B. & ROBERTS, W. W. 1997 A Comparative Study of Computational Methods in Cosmic Gas Dynamics. In *Upwind and High-Resolution Schemes* (ed. M. Y. Hussaini, B. van Leer & J. Van Rosendale), pp. 95–103. Berlin, Heidelberg: Springer.
- ARDAVAN-RHAD, H. 1970 The decay of a plane shock wave. *Journal of Fluid Mechanics* **43** (4), 737–751.
- BARENBLATT, G I & ZEL'DOVICH, Y B 1972 Self-Similar Solutions as Intermediate Asymptotics. *Annual Review of Fluid Mechanics* **4** (1), 285–312.
- BEST, J. P. 1991 A generalisation of the theory of geometrical shock dynamics. *Shock Waves* **1** (4), 251–273.
- BRINKLEY, S. R. & KIRKWOOD, J. G. 1947 Theory of the Propagation of Shock Waves. *Physical Review* **71** (9), 606–611.
- BURNSIDE, R. R. & MACKIE, A. G. 1965 A Problem in shock wave decay. *Journal of the Australian Mathematical Society* **5** (2), 258–272.

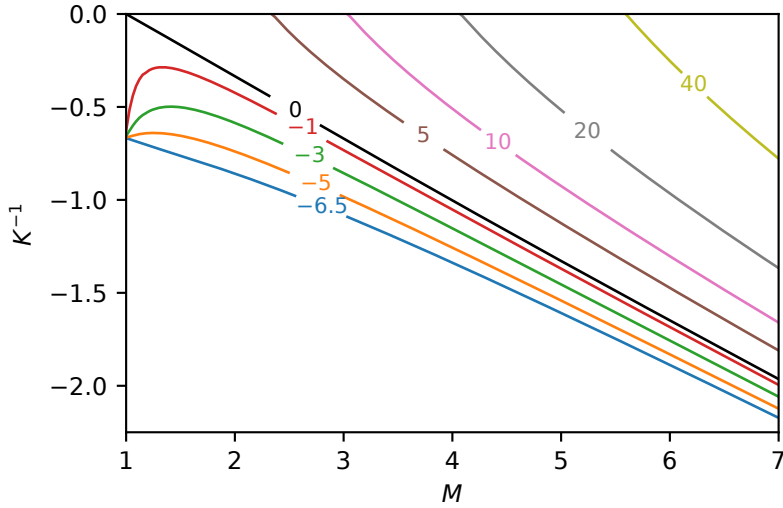


Figure 24: Effect of  $Q$  on  $K^{-1}$  for  $\gamma = 1.2$

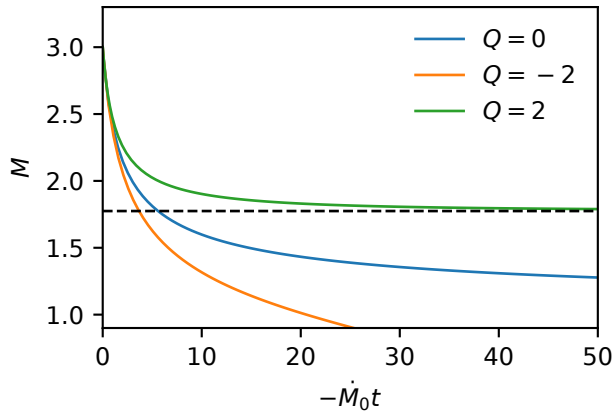


Figure 25: Solutions of shock decay model for  $M_0 = 3$ ,  $\dot{M}_0 = -1$ , and  $\gamma = 1.2$  with nonzero values for  $Q$ . The dashed line is the CJ Mach number for  $Q = 2$  and is  $M_{CJ} = 1.77$

- CASSEN, B. & STANTON, J. 1948 The Decay of Shock Waves. *Journal of Applied Physics* **19** (9), 803–807.
- CHANDRASEKHAR, S. 1943 On the Decay of Plane Shock Waves. *Tech. Rep. No. 423*. Aberdeen Proving Ground.
- CHEN, P. J. & GURTIN, M. E. 1971 Growth and Decay of One-Dimensional Shock Waves in Fluids with Internal State Variables. *Phys. Fluids* **14** (6), 1091–1094.
- CHESTER, W. 1954 CXLV. The quasi-cylindrical shock tube. *The London, Edinburgh, and Dublin Philosophical Magazine and Journal of Science* **45** (371), 1293–1301.
- CHISNELL, R. F. 1957 The motion of a shock wave in a channel, with applications to cylindrical and spherical shock waves. *Journal of Fluid Mechanics* **2** (3), 286–298.
- COTTET, F. & ROMAIN, J. P. 1982 Formation and decay of laser-generated shock waves. *Physical Review A* **25** (1), 576–579, publisher: American Physical Society.

- ECKETT, C. A., QUIRK, J. J. & SHEPHERD, J. E. 2000 The role of unsteadiness in direct initiation of gaseous detonations. *J. Fluid Mech.* **421**, 147–183.
- EILERS, P. H. C. 2003 A perfect smoother. *Analytical Chemistry* **75** (14), 3631–3636.
- FICKETT, W. & DAVIS, W. C. 1979 *Detonation*. Berkeley: University of California Press.
- FOWLES, G. R. 1960 Attenuation of the shock wave produced in a solid by a flying plate. *Journal of Applied Physics* **31** (4), 655–661.
- FRIEDLANDER, F. D. 1958 *Sound Pulses*. Cambridge University Press.
- FRIEDRICHS, K. O. 1948 Formation and decay of shock waves. *Communications on Pure and Applied Mathematics* **1** (3), 211–245.
- GOODWIN, D. G., MOFFAT, H. K. & SPETH, R. L. 2021 Cantera: An Object-oriented Software Toolkit for Chemical Kinetics, Thermodynamics, and Transport Processes. <https://www.cantera.org>.
- GREENSHIELDS, C. 2021 *OpenFOAM v9 User Guide*. London, UK: The OpenFOAM Foundation.
- HENDERSON, SEAN J & MENART, JAMES A 2008 Equilibrium properties of high-temperature air for a number of pressures. *Journal of Thermophysics and Heat Transfer* **22** (4), 718–726.
- HENSHAW, W. D., SMYTH, N. F. & SCHWENDEMAN, D. W. 1986 Numerical shock propagation using geometrical shock dynamics. *Journal of Fluid Mechanics* **171**, 519–545.
- HEYLMUN, J., VONK, P. & BREWER, T. 2021 blastFoam version 5.0 User Guide. <https://github.com/synthetic-technologies/blastofoam>.
- JACKSON, SCOTT I. & SHORT, MARK 2013 The influence of the cellular instability on lead shock evolution in weakly unstable detonation. *Combustion and Flame* **160** (10), 2260–2274.
- JIANG, Z. L., ZHAO, W., WANG, C. & TAKAYAMA, K. 2002 Forward-Running Detonation Drivers for High-Enthalpy Shock Tunnels. *AIAA Journal* **40** (10), 2009–2016.
- KAO, S. T., ZIEGLER, J. L., BITTER, N. P., SCHMIDT, B. E., LAWSON, J. & SHEPHERD, J. E. 2020 SDToolbox: Numerical Tools for Shock and Detonation Wave Modeling. GALCIT Report FM2018.001. California Institute of Technology, Pasadena, CA.
- KOROBENIKOV, V. P. 1991 *Problems of Point-Blast Theory*. New York: American Institute of Physics.
- KURGANOV, A., NOELLE, S. & PETROVA, G. 2001 Semidiscrete Central-Upwind Schemes for Hyperbolic Conservation Laws and Hamilton–Jacobi Equations. *SIAM J. Sci. Comput.* **23** (3), 707–740.
- LANDAU, L. D. & LIFSHITZ, E. M. 1987 *Course of Theoretical Physics-Vol. 6, Fluid Mechanics*, 2nd edn. Pergamon Press.
- LEE, J. H. S. 2016 *The Gas Dynamics of Explosions*. Cambridge University Press.
- VAN LEER, B. 1974 Towards the ultimate conservative difference scheme. II. Monotonicity and conservation combined in a second-order scheme. *Journal of Computational Physics* **14** (4), 361–370.
- MCBRIDE, BONNIE J., ZEHE, MICHAEL J. & GORDON, SANFORD 2002 NASA Glenn coefficients for calculating thermodynamic properties of individual species. Technical Memorandum NASA/TP-2002-211556. NASA Glenn Research Center.
- OSHIMA, K., SUGAYA, K., YAMAMOTO, M. & TOTOKI, T. 1965 Diffraction of a plane shock wave around a corner. *Tech. Rep.* 393. ISAS.
- PEACE, J. T. & LU, F. K. 2018 On the propagation of decaying planar shock and blast waves through non-uniform channels. *Shock Waves* **28** (6), 1223–1237.
- PERT, G. J. 1980 Self-similar flows with uniform velocity gradient and their use in modelling the free expansion of polytropic gases. *Journal of Fluid Mechanics* **100** (2), 257–277.
- RADULESCU, M. I. 2020 On the shock change equations. *Phys. Fluids* **32** (5), 056106.
- RIDOUX, J., LARDIANE, N., MONASSE, L. & COULOUVRAT, F. 2019 Beyond the limitation of geometrical shock dynamics for diffraction over wedges. *Shock Waves* **29** (6), 833–855.
- ROŚACISZEWSKI, JAN 1960 Calculations of the motion of non-uniform shock waves. *Journal of Fluid Mechanics* **8** (3), 337–367.
- SACHDEV, P. L. 2004 *Shock Waves & Explosions*, 1st edn. Chapman and Hall/CRC.
- SCHOEFFLER, D. T. & SHEPHERD, J. E. 2023a Analysis of shock wave acceleration from normal detonation reflection. *Shock Waves* **33**, 205–222.
- SCHOEFFLER, D. T. & SHEPHERD, J. E. 2023b Decay of shock waves in detonation-driven shock tubes. In *34th International Symposium on Shock Waves*, , vol. 2.
- SHARMA, V. D. & RADHA, CH. 1994 On one-dimensional planar and nonplanar shock waves in a relaxing gas. *Phys. Fluids* **6** (6), 2177–2190.
- SHARMA, V. D., RAM, RISHI & SACHDEV, P. L. 1987 Uniformly valid analytical solution to the problem of a decaying shock wave. *Journal of Fluid Mechanics* **185**, 153–170.

- SINGH, MAYANK & ARORA, RAJAN 2021 Propagation of one-dimensional planar and nonplanar shock waves in nonideal radiating gas. *Physics of Fluids* **33** (4), 046106.
- SKEWS, B. W. 1967 The shape of a diffracting shock wave. *Journal of Fluid Mechanics* **29** (2), 297–304.
- TAYLOR, G. I. 1939 The propagation and decay of blast waves. In *The Scientific Papers of Sir Geoffrey Ingram Taylor* (ed. G. K. Batchelor), p. 221. Cambridge University Press.
- THOMPSON, P. A. 1971 A Fundamental Derivative in Gasdynamics. *The Physics of Fluids* **14** (9), 1843–1849.
- THOMPSON, P. A. 1972 *Compressible Fluid Dynamics*. New York: McGraw-Hill.
- VINCENTI, V. G. & KRUGER, C. H. 1965 *Introduction to Physical Gas Dynamics*. New York: Wiley.
- WHITHAM, G. B. 1958 On the propagation of shock waves through regions of non-uniform area or flow. *J. Fluid Mech.* **4** (4), 337–360.
- WHITHAM, G. B. 1999 *Linear and Nonlinear Waves*. John Wiley & Sons, Ltd.
- WOODWARD, P. & COLELLA, P. 1984 The numerical simulation of two-dimensional fluid flow with strong shocks. *Journal of Computational Physics* **54** (1), 115–173.
- WRIGHT, T. W. 1976 An Intrinsic Description of Unsteady Shock Waves. *The Quarterly Journal of Mechanics and Applied Mathematics* **29** (3), 311–324.
- YOUSAF, M. 1974 The effect of overtaking disturbances on the motion of converging shock waves. *Journal of Fluid Mechanics* **66** (3), 577–591.
- YOUSAF, M. 1982 Effect of overtaking disturbances on the motion of a shock wave due to an intense explosion. *The Physics of Fluids* **25** (1), 45–47.
- ZEL'DOVICH, Y. & RAIZER, Y. P. 1967 *Physics of Shock Waves and High Temperature Hydrodynamic Phenomena*. Academic Press.